Atmos. Meas. Tech., 14, 5913–5923, 2021
https://doi.org/10.5194/amt-14-5913-2021

Atmospheric Measurement Techniques
Open Access
EGU

Effects of aerosol size and coating thickness on the molecular detection using extractive electrospray ionization

Chuan Ping Lee[1], Mihnea Surdu[1], David M. Bell[1], Houssni Lamkaddam[1], Mingyi Wang[2,3], Farnoush Ataei[4], Victoria Hofbauer[2,3], Brandon Lopez[2,5], Neil M. Donahue[2,3,5,6], Josef Dommen[1], Andre S. H. Prevot[1], Jay G. Slowik[1], Dongyu Wang[1], Urs Baltensperger[1], and Imad El Haddad[1]

[1]Laboratory of Atmospheric Chemistry, Paul Scherrer Institute, 5232 Villigen, Switzerland
[2]Center for Atmospheric Particle Studies, Carnegie Mellon University, Pittsburgh, PA 15213, USA
[3]Department of Chemistry, Carnegie Mellon University, Pittsburgh, PA 15213, USA
[4]Department of Experimental Aerosol and Cloud Microphysics, Leibniz Institute for Tropospheric Research, 04318 Leipzig, Germany
[5]Department of Chemical Engineering, Carnegie Mellon University, Pittsburgh, PA 15213, USA
[6]Department of Engineering and Public Policy, Carnegie Mellon University, Pittsburgh, PA 15213, USA

Correspondence: Imad El Haddad (imad.el-haddad@psi.ch), Dongyu Wang (dongyu.wang@psi.ch), and Jay G. Slowik (jay.slowik@psi.ch)

Received: 29 January 2021 – Discussion started: 6 April 2021
Revised: 7 July 2021 – Accepted: 9 July 2021 – Published: 2 September 2021

Abstract. Extractive electrospray ionization (EESI) has been a well-known technique for high-throughput online molecular characterization of chemical reaction products and intermediates, detection of native biomolecules, in vivo metabolomics, and environmental monitoring with negligible thermal and ionization-induced fragmentation for over two decades. However, the EESI extraction mechanism remains uncertain. Prior studies disagree on whether particles between 20 and 400 nm diameter are fully extracted or if the extraction is limited to the surface layer. Here, we examined the analyte extraction mechanism by assessing the influence of particle size and coating thickness on the detection of the molecules therein. We find that particles are extracted fully: organics-coated NH_4NO_3 particles with a fixed core volume (156 and 226 nm in diameter without coating) showed constant EESI signals for NH_4NO_3 independent of the shell coating thickness, while the signals of the secondary organic molecules comprising the shell varied proportionally to the shell volume. We also found that the EESI sensitivity exhibited a strong size dependence, with an increase in sensitivity by 1–3 orders of magnitude as particle size decreased from 300 to 30 nm. This dependence varied with the electrospray (ES) droplet size, the particle size and the residence time for coagulation in the EESI inlet, suggesting that the EESI sensitivity was influenced by the coagulation coefficient between particles and ES droplets. Overall, our results indicate that, in the EESI, particles are fully extracted by the ES droplets regardless of the chemical composition, when they are collected by the ES droplets. However, their coalescence is not complete and depends strongly on their size. This size dependence is especially relevant when EESI is used to probe size-varying particles as is the case in aerosol formation and growth studies with size ranges below 100 nm.

1 Introduction

Atmospheric aerosols are suspended particles in the air ranging from a few nanometers (nm) to several micrometers (µm) in diameter. Fine particles (< 1 µm) comprise nucleation, Aitken and accumulation mode particles and can account for 50 %–70 % of the total particulate matter (PM) mass concentration in polluted environments (Yue et al., 2009). They can affect the earth's radiative balance either directly, by interacting with solar radiation, or indirectly by acting as cloud condensation nuclei (CCN), influencing cloud albedo and lifetime (Seinfeld and Pandis, 2016). Exposure to PM is one of the leading causes of premature death, accounting

for ∼ 8.9 million deaths, or ∼ 10 % of total global burden of mortality in 2015 (Burnett et al., 2018), though the underlying mechanisms remain uncertain (Daellenbach et al., 2020). PM can be emitted as primary aerosol or produced in the atmosphere after chemical reactions via nucleation or condensation of gas-phase products (Berndt et al., 2005; Clarke et al., 1984; Hoffmann et al., 1997; Jimenez et al., 2009; Kalberer et al., 2004; Kirkby et al., 2011). Heterogeneous reactions may also further increase the complexity of ambient aerosol mixtures (George and Abbatt, 2010; Ditto et al., 2020).

Online molecular characterization of atmospheric aerosols is required to resolve the spatiotemporal variability of PM molecular composition and to identify PM sources. Progress has been made with the development of chemical ionization interfaces such as the Filter Inlet for Gases and AEROsols (FIGAERO) (Lopez-Hilfiker et al., 2014), Thermal Desorption Differential Mobility Analyzer (TD-DMA) (Holzinger et al., 2010; Wagner et al., 2018), and Chemical Analysis of Aerosol Online (CHARON) (Eichler et al., 2015) coupled to a mass spectrometer. However, these techniques suffer from thermal decomposition of the analyte prior to ionization and/or ionization-induced fragmentation, impeding molecular speciation (Müller et al., 2017; Stark et al., 2017). To complement these instruments, an extractive electrospray (ES) ionization time-of-flight mass spectrometer (EESI-TOF) was developed to enable molecular characterization of organic aerosol at 1 Hz time resolution with ng m^{-3} level detection limit, as well as minimal thermal and ionization-induced fragmentation (Lopez-Hilfiker et al., 2019). The EESI-TOF was further developed to enable online tandem mass spectrometry for molecular structure elucidation and to characterize water-soluble metals (Giannoukos et al., 2020; Lee et al., 2020).

Several studies on topics such as the extraction of macromolecules from colloidal solution (Chen et al., 2006), electron-transfer-catalyzed dimerization (Marquez et al., 2008), and gas plume mixing in the charged droplets (Cheng et al., 2008) reported that the ionization of EESI mainly happens in the liquid phase via interaction between charged ES droplets and neutral analyte molecules. For clarity, we refer to our analytes (here introduced in aerosol form) as "particles" prior to their interaction with ES droplets and as "analyte-laden droplets" afterwards. If this liquid-phase extraction of EESI occurs via total coalescence between particles and ES droplets, the measured EESI signal should be proportional to the total analyte mass concentration, i.e., full extraction of particles by ES droplets as demonstrated by several studies (Law et al., 2010; Lopez-Hilfiker et al., 2019). In contrast, prior studies suggested that the particles may be only partially probed, limiting the full quantification of the extracted analyte with extractive electrospray ionization (Wang et al., 2012, Kumbhani et al., 2018). Kumbhani et al. (2018) suggested that only the surface of particles with a diameter of approximately 100 nm was extracted by comparing infusion ESI-MS with EESI-MS using coated chemical standards (Kumbhani et al., 2018). Using other techniques such as phase Doppler anemometer, Wang et al. (2012) suggested that the extraction happens via fragmentation of the analyte droplets and ES droplets as the result of droplet–droplet collisions (Wang et al., 2012). Finally, other studies proposed that the EESI extraction efficiency could depend on the analyte volatility and size (Meier et al., 2011; Pagonis et al., 2021). Since all these studies only probed simple systems, i.e., individual chemical standards using one kind of experimental setup and EESI ionization source, these discrepancies could be inherently attributed to their differences of ES ionization geometries, experimental conditions, irreproducible ES Taylor cone conditions and perhaps the choices of chemicals.

Without reconciling the discrepancies of these reported EESI mechanisms, EESI quantification must be regarded as highly uncertain when the technique is used to probe varying size distributions of particles that exist in different mixing states and are comprised of different molecular polarity, volatility and sizes. Here, we took advantage of recent advancements in particle generation and chemical analysis to evaluate the extraction mechanism of EESI using three different methods for particle generation and several online mass spectrometers for aerosol chemical speciation. First, we characterized the EESI extraction efficiency with particles containing atmospherically relevant standard compounds and mixtures, size-selected in the range of 30–500 nm using an aerosol aerodynamic classifier. We elucidated the influence of ES operating parameters and the residence time of ES droplets and particles within the ionization source using two different EESI sources. Second, we assessed whether the EESI extraction efficiency depends on the analyte chemical composition, by comparing the EESI-TOF with a chemical ionization (CI) TOF-MS equipped with a Filter Inlet for Gases and AEROsols (FIGAERO) sampling manifold (FIGAERO-CI-TOF-MS) during measurements of α-pinene secondary organic aerosol (SOA) generated in the CLOUD (Cosmics Leaving OUtdoor Droplets) chamber at CERN, Switzerland (Kirkby et al., 2016; Tröstl et al., 2016; Dias et al., 2017). Third, we determined whether particles are fully extracted or if extraction is limited to the coated surface by coating monodisperse NH_4NO_3 particles of a fixed size with variable amounts of oxidation products in an oxidation flow tube reactor.

2 Experiment

2.1 Materials

Acetonitrile (Sigma-Aldrich, UV grade), sodium iodide (Sigma-Aldrich, 99.7 % purity) and Milli-Q water (18 MΩ cm) were used to prepare the electrospray (ES) and chemical standard nebulization solution. A polyimide-

coated fused silica capillary (inner diameter (i.d.): 75 µm, outer diameter (o.d.): 369 µm; BGB Analytik, Böckten, Switzerland), HEPA capsule filter (Pall Corporation), PEEK tubing (i.d.: 500 µm, o.d.: 1/16 in.; BGB Analytik, Böckten, Switzerland) and charcoal denuders (Ionicon GmbH, Austria) were used for the electrospray ionization inlet. As chemical standards, α-pinene (Sigma-Aldrich, 99 % purity), levoglucosan (Sigma-Aldrich, 99 % purity), sucrose (Sigma-Aldrich, 99 % purity) and ammonium nitrate (Sigma-Aldrich, 98 % purity) were used.

2.2 Electrospray ionization configuration

Two designs of the EESI sources with a factor of 2 difference in their residence time in the electrospray ionization region were used in this work, coupled to a high-resolution TOF mass spectrometer (HTOF, Tofwerk AG, Switzerland). EESI source A (Lopez-Hilfiker et al., 2019) and B were developed initially for Tofwerk TOF and Thermo Scientific Orbitrap mass analyzers (Fig. S1), respectively, though EESI source B is compatible with both mass analyzers, as described in detail elsewhere (Lee et al., 2020). Source A was used throughout the study, and source B was only used in size-selection experiments shown in Fig. 2. Two electrospray (ES) solutions were used to generate charged ES droplets: (1) acetonitrile/H_2O (50/50 v/v) and (2) 100 % H_2O (Table S1). Both solutions were doped with 100 ppm NaI. A potential difference of around 2.6–2.9 kV relative to the MS interface was applied to the ES solution, and an air pressure difference of 120 to 800 mbar was applied to the ES solution bottle reservoir, delivering 0.3–23 µL min^{-1} of ES solution via a polyimide fused silica capillary (o.d.: 369 µm and i.d.: 50, 75 and 100 µm, BGB Analytik, Switzerland). Different ES operating parameters with estimated ES parent droplet sizes ranging from 0.7 to 5.66 µm are tabulated in Table S2. The ES droplets intersected with the particles before entering the heated TOF capillary kept at 275 °C (< 1 ms residence time), undergoing a Coulomb explosion as the ES droplets evaporated. The ions generated from organic molecules were detected predominantly (> 95 % relative abundance) as sodiated adducts ($[M+Na]^+$) in the positive ionization mode by the HTOF. Ammonium nitrate (NH_4NO_3), an inorganic salt, was detected as $[NaNO_3+Na]^+$. The raw mass spectra (1 Hz) were post-averaged every 10 s using Tofware (version 2.5.13). All measured analyte signals were normalized by the most abundant electrospray ion (i.e., $[NaI+Na]^+$) to account for the variation of the electrospray signal (±5 %).

2.3 Particle size selection

Figures S2 and S3 show two experimental setups for the investigation of the size dependence of the particle extraction efficiency using EESI. Chemical standards were used in the first experimental setup (Fig. S2). Three individual aqueous solutions containing 4000 ppm of levoglucosan, sucrose and ammonium nitrate, respectively, were nebulized separately at 1.4 L min^{-1}, which was then mixed with a 1.6 L min^{-1} make-up zero air. The output particles were dried with a custom-made drier containing silica gel (<5 % RH) and subsequently size-selected using an aerosol aerodynamic classifier (AAC; Cambustion, United Kingdom) to produce monodisperse particles (Tavakoli and Olfert, 2013, 2014; Tavakoli et al., 2014). The size selection was implemented by centrifugal separation of the particles according to their mass. Unlike size selection using differential mobility analyzers (Lopez-Hilfiker et al., 2019), size selection using the AAC does not require electrical charging, thereby avoiding multi-charging artifacts. The possible multi-charging of particles might affect the normal extraction condition by EESI where the particles are assumed to be neutral (Kebarle and Verkcerk, 2009, 2012). In addition, doubly charged particles could result in underestimation of particle size and mass concentration. Therefore, the new experimental setup we used here was well suited to study the size dependence of EESI sensitivity.

After particle size selection, the sample was drawn through a multichannel charcoal denuder to strip gas-phase constituents before entering the EESI-TOF inlet manifold. The sample was also characterized immediately upstream of the electrospray region by a nano-scanning mobility particle sizer (size range 2.5–239 nm, nano-SMPS, TSI Inc., USA), a scanning mobility particle sizer (size range 16–638 nm, TSI SMPS, TSI Inc., USA) and an aerosol mass spectrometer equipped with a long time-of-flight mass analyzer (AMS-LTOF, Aerodyne Research Inc., USA) (Fig. S2). The high concentration of the chemical solutions ensured that sufficiently high analyte concentrations (>3 µg m^{-3}) remain after size selection by the AAC using the highest possible sheath flow (15 L min^{-1} at an aerodynamic diameter D_{ae}>150 nm) to produce highly monodisperse particle distributions (Tavakoli and Olfert, 2014) at 30 %–40 % RH. A HEPA filter was used for the background measurements after each particle size selection.

In the second configuration (Fig. S3), we investigated the size-dependent EESI sensitivity towards biogenic SOA produced from α-pinene oxidation in the Cosmic Leaving OUtdoor Droplets (CLOUD) chamber at CERN, Switzerland (Kirkby et al., 2011; Dias et al., 2017), at −50 to −30 °C with 20 % and 60 % RH (Simon et al., 2020). The EESI-TOF signals of individual α-pinene oxidation products ($C_{10}H_{16}O_{3-8}$) were compared to a FIGAERO-CI-TOF-MS (Lopez-Hilfiker et al., 2014). The FIGAERO-CI-TOF-MS measured both the gas and particle phases. Here, particles were first collected onto a 24 mm diameter PTFE filter via a dedicated port with a sampling flow rate of 6 L min^{-1}. Then, 2.7 L min^{-1} of ultra high purity (UHP) N_2 was heated progressively to thermally desorb and vaporize the collected particles during a 14 min desorption period, with the filter temperature varying from 20 to 150 °C at a rate of 10 °C min^{-1}. The desorbed vapor analytes were sampled into an ion–molecule

reactor at 150 mbar and chemically ionized by iodide (I^-) ions generated by passing a UHP N_2 gas stream containing CH_3I through a ^{210}Po radioactive source before entering an LTOF mass analyzer for separation. The signal of the FIGAERO-CI-TOF-MS was integrated over the period of particle desorption. The organic analytes were detected predominantly in the form of iodide adducts $[M+I]^-$ (>95 % relative abundance). The sample collection efficiency of the filter used by the FIGAERO-CI-TOF-MS is expected to be higher than 99.9 % for particles above 10 nm (Hilfiker-Lopez et al., 2014). The volume-weighted geometric mean diameters were determined using an SMPS (size range 9–834 nm, Leibniz Institute for Tropospheric Research, Germany). The SMPS(s) used for the measurements of chemical standards and α-pinene SOA was (were) calibrated using size standards of polystyrene latex beads.

2.4 Particle surface coating

A 104 cm long Pyrex flow tube of 7.4 cm inner diameter with a total volume of approximately 5 L (Molteni et al., 2018) was used for particle surface coating experiments (Fig. S4). A 1000 ppm NH_4NO_3 solution in pure water was nebulized at 1.4 L min^{-1} and dried before size selection by the AAC (<5 % RH). The resulting NH_4NO_3 particles passed through the charcoal denuders before entering concentrically into the flow tube with a laminar zero air sheath flow of 10 L min^{-1} at 20 °C and 60 % RH. Measurements were performed downstream of the flow tube. Particle composition and size were measured by the EESI-TOF and SMPS (16–615 nm), respectively. Two different core sizes (155.8 and 226.4 nm) of NH_4NO_3 particles were used for the coating experiments; 4.7 ± 0.4 ppm α-pinene, as measured by a quadrupole proton-transfer-reaction mass spectrometer (Q-PTR), was injected into the flow tube from a glass vial with a zero air carrier flow (1 L min^{-1}). To generate ozone, 20–200 mL min^{-1} zero air (60 % RH at 20 °C) was irradiated by an amalgam lamp (185 and 254 nm; WISAG GmbH, Switzerland). Ozone was mixed with α-pinene to produce ozonolysis products which condensed onto, i.e., "coated", the NH_4NO_3 particles inside the flow tube. Note that depending on the conditions, this coating may either result in a core-shell structure or in the formation of a homogeneous single phase, though the exact morphology does not affect the conclusion regarding surface extraction, as discussed below. The coating period in the flow tube was approximately 26 ± 0.5 s. The coating thickness was controlled by varying the ozone concentration in the presence of excess α-pinene, which was measured by a Thermo 49A ozone analyzer (Thermo Fisher Scientific, USA) to be 20–310 ppb. This ozone concentration range was optimized before injecting the NH_4NO_3 particles to ensure that no nucleation occurred which would have resulted in particles consisting only of SOA. At the beginning of each ozone concentration step, the EESI-TOF sampled the gas and aerosol mixture through a bypass channel without denuder to ensure that all oxidation product signals reached steady state (<20 min). Afterwards, routine sampling alternated between filtered background (5 min) and particle-phase measurements (10 min). This coating experiment was carefully designed to achieve high condensational growth rates of about 0.8 nm s^{-1} with negligible nucleation.

3 Results and discussion

3.1 Influence of particle size on EESI-TOF detection

Figure 1a shows a typical measurement of the EESI-TOF and SMPS for size-selected sucrose particles. Two sheath flow rates (5 and 15 L min^{-1}) at 1.4 L min^{-1} of particle flow rate were used to generate size-selected sucrose particle distributions with a geometric standard deviation σ_g of 1.4 and 1.2, respectively. A comparison of the signals in the red windows in Fig. 1b shows that the sucrose signal did not increase commensurately with the mass concentration measured by the SMPS (regardless of σ_g), as the volumetric geometric mean diameter of the particles increased. To quantify this effect, we define the size-dependent sensitivity $S(D_P)$ as

$$S(D_P) = \frac{I(D_P)}{M(D_P)}, \quad (1)$$

where $I(D_P)$ is the peak intensity of the analyte (Fig. 2) or the total intensity of fitted organic ions (Fig. 3a) that is normalized by the most abundant electrospray ion ($[NaI+Na]^+$) to account for the ES fluctuation (<5 %); $M(D_p)$ is the mass concentration of the particles measured by the SMPS or/and by the AMS-LTOF as a function of the volumetric geometric mean mobility diameter D_P. To show the relative change of the sensitivity as a function of D_P, $S(D_P)$ is normalized by its value at 100 nm electrical mobility diameter, defined as the normalized sensitivity, $S_{100\,nm}$:

$$S_{100\,nm} = \frac{S(D_P)}{S(D_P = 100\,nm)}. \quad (2)$$

The normalization by the sensitivity at 100 nm, $S(D_p = 100\,nm)$, was chosen to accommodate and compare all datasets in this study. The value of $S(D_p = 100\,nm)$ was interpolated by fitting a three-parameter function $S(D_P, P_1, P_2, P_3) = P_1 \cdot D_p{}^{\wedge}(P_2) + P_3$ to $S(D_p)$.

We investigated the normalized sensitivities of the EESI-TOF for levoglucosan, sucrose and NH_4NO_3 (tracers of biomass and anthropogenic activities in the ambient atmosphere) using different EESI ionization sources and ES operating parameters that resulted in different ES parent droplet diameters as estimated in Tables S1, S2 and S3. Figure 2 shows the normalized sensitivity of size-selected particles, $S_{100\,nm}$ (Eq. 2) as a function of the volumetric geometric mean diameter of the particles generated using both pure component and mixed solutions detected under different ES conditions (see also Fig. S6, Tables S1–S3). The $S_{100\,nm}$ for

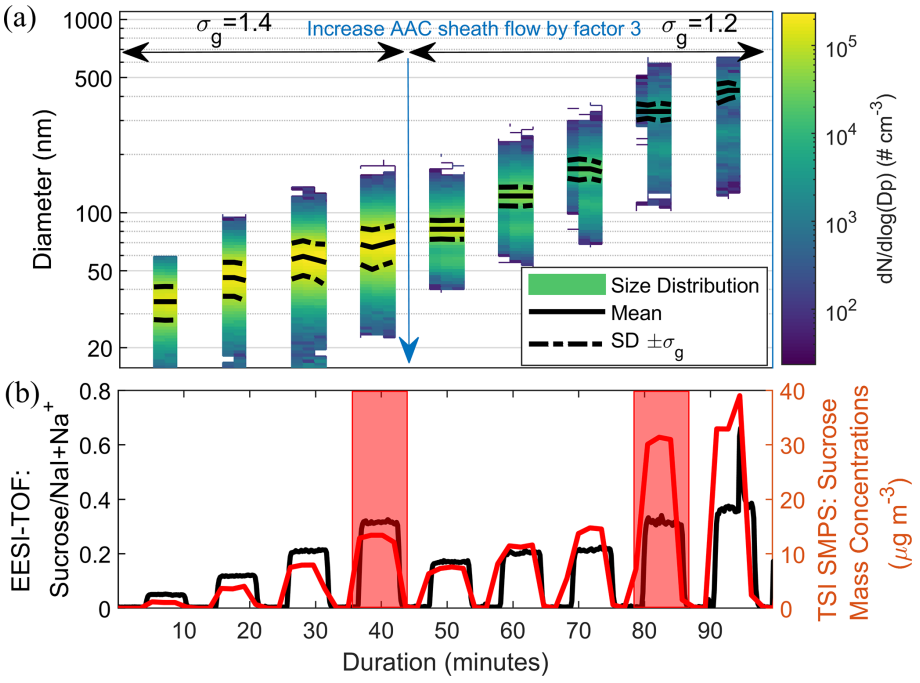

Figure 1. **(a)** Number-weighted size distribution of sucrose particles as measured by the SMPS after size selection using the AAC at two different settings of the AAC sheath flow. The solid and dashed black lines denote the geometric mean and ± 1 geometric standard deviation, σ_g, of the number-weighted size distributions, respectively. The geometric standard deviation of the size-selected particle distribution of sucrose is lower at the higher sheath flow of the AAC as expected. Data points of particle counts lower than 1 cm^{-3} were removed. See Fig. S5 for the size-selection performance of the AAC as measured by the SMPS. **(b)** A representative EESI-TOF measurement that shows the time series of sucrose normalized to the $[NaI + Na]^+$ signal (most abundant ES ion) and the corresponding integrated particle mass concentration measured by the SMPS for size-selected sucrose particles (using the integrated volume concentration and a density of 1.59 g cm^{-3}). Red windows indicate periods with the similar EESI signal intensity of sucrose but different particle size and mass concentration.

different types of particles decreased by up to 3 orders of magnitude as the volumetric geometric mean diameter increased from 30 to 300 nm, with some approaching a plateau at larger particle sizes. The size-dependent sensitivity is observed for both single compounds and compound mixtures (Fig. S6).

Assuming that the detected ions from the size-selected particles by EESI are generated after coagulation and extraction between the particles and ES droplets, the normalized sensitivity $S_{100\,nm}$ should be proportional to the total coagulated mass. The determination of the total coagulated mass requires a Brownian coagulation coefficient (BCC, computed from the particle and ES droplet size), the number concentrations and the residence time. However, the actual ES droplet size distribution could not be measured using other physical processes because these additional processes could alter the ES droplets properties and affect the electrospray ionization. Therefore, we could only calculate the BCC for different size-selected monodisperse particles assuming ES parent droplet sizes of 0.5, 1.5 or 5 µm. These three chosen ES parent droplet sizes represent the likely range of the actual ES droplet sizes, which is theoretically estimated from our ES operating parameters as summarized in Table S2, based on Supplement Eqs. (S3)–(S6) and Fig. S7. The calculated BCC values were normalized to the BCC for 100 nm monodisperse particles, denoted as $BCC_{100\,nm}$, as shown in Fig. S6a, analogous to the normalization for $S_{100\,nm}$. Most normalized sensitivities (i.e., normalized total coagulated masses) correlate well with the $BCC_{100\,nm}$, as shown in Fig. 2. Smaller particles have a higher BCC and are collected more efficiently, contributing a higher percentage of their total mass to the analyte-laden ES droplets during extraction. Furthermore, the plateaus of $S_{100\,nm}$ at larger particle sizes could be explained by the suggested behavior of $BCC_{100\,nm}$ when the size of the particle is similar to the actual ES droplet size or partly to the estimated ES parent droplet size in our study. The high deviation of size-dependent sensitivity ($\sim 50\,\%$) for $D_p > 200$ nm is likely due to the variation of the actual ES droplet size distribution in different calibration runs, which can deviate from the estimated ES parent droplet size. Knowledge of the actual ES droplet size distribution is needed to further explain the variabilities but are beyond the scope of the current study.

It is intuitive that the total coagulated mass for extraction is also dependent on the residence time for coagulation between the particles and the ES droplets during electrospray ioniza-

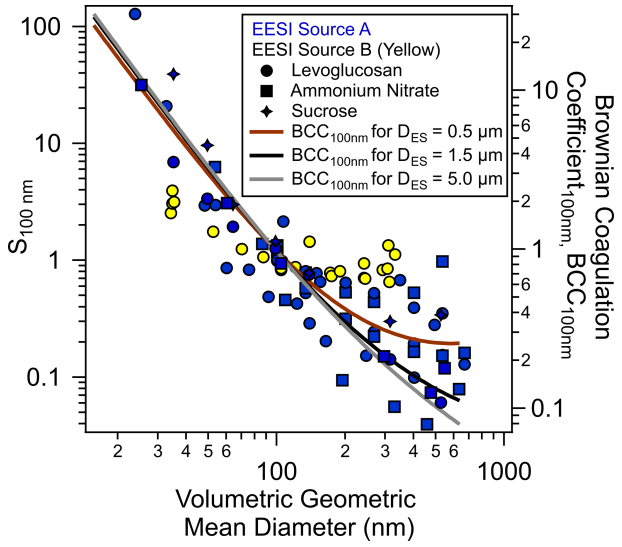

Figure 2. Sensitivities of the EESI-TOF towards various standards normalized to their respective values at 100 nm as a function of the particle volumetric geometric mean diameter. Blue and yellow markers indicate EESI sources A and B, which were initially developed for TOF and Orbitrap mass analyzers, respectively (Lopez-Hilfiker et al., 2019; Lee et al., 2020). Different marker types (●), (■), (✦) denote levoglucosan, NH_4NO_3 and sucrose, respectively. The Brownian coagulation coefficients are calculated using the range of ES parent droplet sizes estimated based on our ES operating parameters (Figs. S6 and S7). Note that some of the data points may overlap at the similar volumetric geometric mean diameter due to repetitions of the same experiment settings.

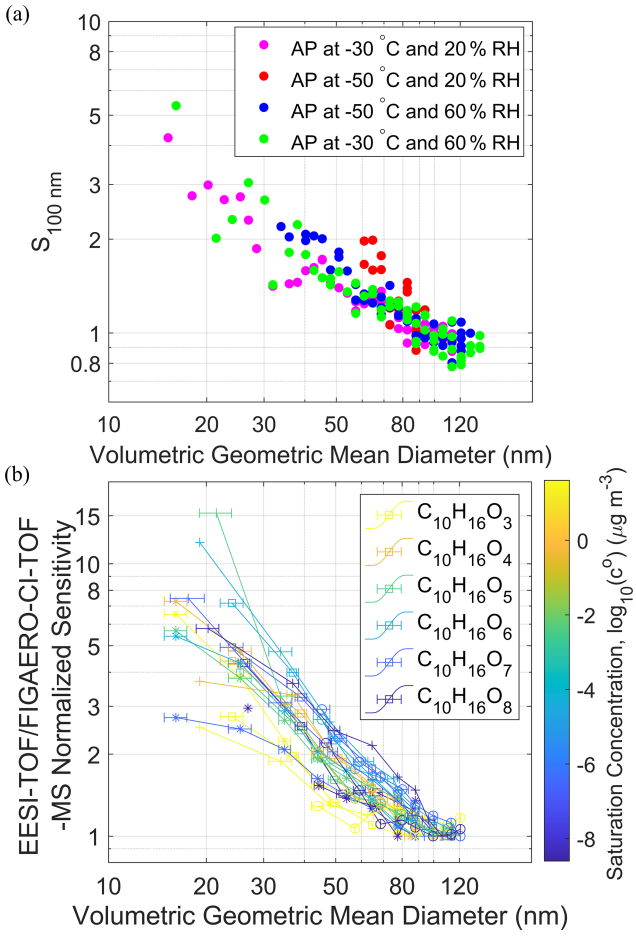

Figure 3. (a) Normalized sensitivity of the EESI-TOF calculated from the sum of high-resolution fitted organic ion signals and the total particle mass concentrations as a function of the volumetric geometric mean diameter over the course of new particle formation and growth of α-pinene (AP) ozonolysis SOA. See Figs. S8, S9 and S10 for more information. **(b)** Normalized sensitivity of the EESI-TOF intensity divided by the FIGAERO-CI-TOF-MS intensity for $C_{10}H_{16}O_{3-8}$ molecules in the particle phase as a function of the volumetric geometric mean diameter. Different marker types □, ∗, ◯, + indicate different SOA formation conditions, i.e., at −30 °C and 20 % RH, −50 °C and 20 % RH, −50 °C and 60 % RH, −30 °C and 60 % RH, respectively. The saturation concentration was estimated as $\log_{10}(c^0) = (n_c^0 - n_c)b_c - n_o b_o - 2 \cdot b_{co}(n_c n_o)/(n_c + n_o)$ from the number of carbon and oxygen (n_c, n_o) and coefficients (b_c, b_o, b_{co}) provided in Donahue et al. (2011).

tion. A longer residence time would allow for a higher percentage of the particle total mass to be extracted; i.e., the coagulation of smaller particles would saturate, while the coagulation of larger particles would continue, which would result in a smaller range of size-dependent total coagulated mass (shallower size-dependent sensitivity). We examined this hypothesis by using an EESI source B which provides a factor of 2 longer residence time in the electrospray ionization region. As shown in Fig. 2, the sensitivity size dependence resulting from EESI source B (yellow markers), which has twice the residence time as EESI source A, is significantly shallower than the one from EESI source A (blue markers), consistent with our hypothesis. Overall, Fig. 2 suggests that the size-dependent sensitivity (total coagulated mass) is dependent on the Brownian coagulation coefficient, which varies with the ES droplet size (and therefore ES operating parameters), as well as the residence time for coagulation. Such size dependence suggests that the ionization of analyte particles in the EESI proceeds through coagulation at a certain size-dependent efficiency, e.g., partial coalescence between particles and ES droplets, as reported by the previous studies (Wang et al., 2012; Kumbhani et al., 2018; Pagonis et al., 2020).

Konermann et al. (2013) reported that the electrospray droplet evaporation can be affected by the size and the polarity of analyte molecules, while Meier et al. (2011) suggested that the extraction efficiency of EESI can depend on the volatility of analyte molecules. We investigated the EESI sensitivity size dependence for a complex mixture of internally mixed α-pinene oxidation products formed in the CLOUD chamber, to evaluate whether such dependence varies with analyte volatilities, e.g., if volatile species prefer-

entially evaporate from smaller particles before their subsequent ionization. We generated unimodal size distributions of secondary organic aerosol (SOA) with volumetric geometric mean diameters ranging from 17 to 137 nm (Figs. S8 and S9). Figure 3a shows the normalized sensitivity of the sum of the organic ions measured by the EESI-TOF after high-resolution peak fitting, $S_{100\,\mathrm{nm}}$, as a function of the measured particle size. $S_{100\,\mathrm{nm}}$ decreases from a value of 6 at $D_\mathrm{p} = 17$ nm to ~ 1 at $D_\mathrm{p} = 110$ nm. The change in normalized sensitivity is similar to the results obtained for individual chemical standards presented in Fig. 2 for EESI source A. To examine whether there is a composition dependence on the EESI extraction, we compared the signals of $C_{10}H_{16}O_{3-8}$ compounds measured by the EESI-TOF and the FIGAERO-CI-TOF-MS from SOA produced at different temperatures and RH in the CLOUD chamber as shown in Fig. 3b (see also Fig. S10).

The linear behaviors of different measured species between the EESI-TOF and the FIGAERO-CI-TOF-MS for $17\,\mathrm{nm} < D_\mathrm{p} < 80\,\mathrm{nm}$ in Fig. 3b show that the relative abundances of the sampled aerosol chemical composition are similar and comparable for both instruments with negligible re-volatilization of particles at two different sampling points. Thermal decomposition may affect the absolute quantification of particle-phase compounds by the FIGAERO-CI-TOF-MS (Stark et al., 2017). However, to the best of our knowledge, no size dependence has been reported in the literature for this thermal artifact, which should be canceled after sensitivity normalization comparison in relative scale for each species of FIGAERO-CI-TOF-MS. The sensitivity size dependence appears to be similar for $C_{10}H_{16}O_{3-8}$ compounds with estimated saturation vapor concentrations ranging from $10^{-8.6}$ to $10^{1.6}\,\mu\mathrm{g\,m^{-3}}$. Both results from size-selected chemical standards (Fig. 2) and chemical resolution comparison between EESI-TOF and FIGAERO-CI-TOF-MS using a complex SOA mixture indicate that the EESI sensitivity size dependence is a function of the Brownian coagulation coefficient rather than molecular size, polarity or volatility. Aside from the size dependence, we did not observe any systematic RH influence on the EESI sensitivity for size-selected chemical standards (30 %–40 % RH) and α-pinene SOA (20 % and 60 % RH). This is consistent with the findings by Lopez-Hilfiker et al. (2019), where RH does not systematically affect EESI sensitivity but instead shows molecule-dependent effects where, within an internally mixed particle, the sensitivity of certain molecules may increase with RH while others decrease. The enhancement in EESI sensitivity for wet aerosol over dry aerosol was reported in a previous study (Kumbhani et al., 2018). If EESI extraction is limited to the surface of the analyte aerosol, the aerosol water content may mobilize surface species to facilitate dissolution. However, the lack of RH dependence for our EESI setup indicates that such surface extraction limitation is absent in our study.

3.2 Influence of particle coating thickness on EESI sensitivity

Limited surface extraction, approximately 2–4 nm in depth, of the particles was reported for some ESI source designs (Kumbhani et al., 2018; Wingen and Finlayson-Pitts, 2019). If such an effect were present in the EESI-TOF design used in the current study, it could also appear as a size-dependent sensitivity. This would mean that a smaller fraction of the analyte volume is extracted as the particle diameter increases and that the EESI sensitivity scales with the particle surface area rather than the volume. To determine the potential contribution by surface extraction to the observed sensitivity size dependence, we investigated the extraction efficiency of NH_4NO_3 particles of 156 and 226 nm in diameter before being coated by the α-pinene oxidation products using source A. Source A was chosen because it has the greatest extent of size-dependent sensitivity in comparison to source B. The core NH_4NO_3 sizes were chosen as the size-dependent sensitivity decreases by less than 15 % from 155 nm to 250 nm for single and mixed component particles (Fig. 2). The coating thickness on the NH_4NO_3 particles ranged between 12 and 26 nm, with a coated organic mass concentration up to $31\,\mu\mathrm{g\,m^{-3}}$ (Fig. S11).

If extraction were limited to the particle surface, the EESI signal for NH_4NO_3, i.e., $[NaNO_3 + Na]^+$, should decrease similar to the size-dependent sensitivity (Fig. 2) that is exhibited by source A. For instance, if the coated particles were of core-shell morphology, then the extraction of the NH_4NO_3 core would be limited by the thickness of the organic coating and the ES extraction depth. Alternatively, if the coated particles were homogeneous inorganic–organic mixtures, then the detected NH_4NO_3 signal would still decrease in proportion to the decreasing NH_4NO_3 mass fraction as the condensed organic mass increases. In Fig. 4, we show the signals of NH_4NO_3 and selected organic molecules with low volatility as a function of the coating volume (normalized to their respective minimum coating volume separately for each of the NH_4NO_3 particle core sizes). The coating signal from $C_{10}H_{16}O_{6-8}$ is proportional to the coating volume, whereas the NH_4NO_3 particle signal remains constant with increasing coating thickness for both core sizes (see also Fig. S12). This proportionality also demonstrates that the condensable species as a coating substance is not limited by the mean oxidation states of oxidation products because there is no decrease of the $C_{10}H_{16}O_6$ for an increase of $C_{10}H_{16}O_8$. Our results suggest that there is no surface extraction limitation for particles up to at least 250 nm in diameter for the EESI inlet designs used in the current study. Prior reporting of surface extraction limitation may stem from the specific EESI configuration or experimental method used, which relied on the comparison of EESI and ESI measurements (Kumbhani et al., 2018), where the differences in dissolution/extraction timescale and sample preparation between EESI and ESI techniques could contribute to the discrepancies observed.

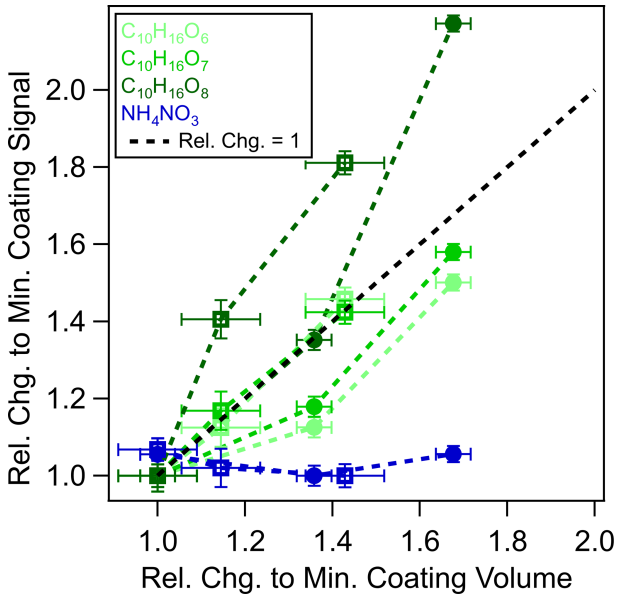

Figure 4. Relative changes of α-pinene ozonolysis products coated on NH_4NO_3 particles at 156 (●) and 226 nm (□) core sizes. The coating volume (x axis) measured by an SMPS is normalized by the smallest coating volume, and the coating signals (y axis) of $C_{10}H_{16}O_{6–8}$ molecules as measured by the EESI-TOF are normalized by the signals observed at the smallest coating volume. The largest coating thicknesses are 19.8 and 26.8 nm for 156 and 226 nm core sizes of the NH_4NO_3 particles, respectively. The black line denotes a relative change of the coating signal and volume equal to 1.

4 Conclusion

We explored the dependence of the EESI sensitivity on particle size using individual chemical standards and chemical mixtures with two different EESI source designs. We show that the EESI sensitivity decreases as the size of the particles increases. The sensitivity size dependence correlates with the Brownian coagulation coefficient and the residence time for coagulation. The results suggest that the particles undergo coalescence with the ES droplets as suggested in previous studies (Law et al., 2010; Wang et al., 2012), but the efficiency of the coalescence is limited by the coagulation coefficient, which depends on the particle and ES droplet sizes. From a comparison with the FIGAERO-CI-TOF-MS online measurements, we show that the EESI sensitivity size dependence is also present for internally mixed secondary organic aerosol made of molecules with volatilities varying by approximately 10 orders of magnitude. While the total extracted mass is related to the size-dependent Brownian coagulation coefficient (i.e., not all particles of different size can coalesce with all the electrospray droplets), coating experiments show that the volume of particles, once coagulated with the ES droplet, is fully extracted up to a size of 250 nm for our EESI configuration instead of limited surface extraction reported by the previous work (Kumbhani et al., 2018). Future work should investigate the EESI response to coarse-mode particles (with $D_p > 1$ µm), elucidate the relationship between size-dependent sensitivity behavior and different chemical mixtures, and search for an optimal residence time for coagulation in the EESI source to achieve the least steep size-dependent sensitivity for the particle size range of interest. EESI users should be cognizant of the size-dependent sensitivity during their experiment design and data analysis. Such size dependence is especially relevant when studying aerosol formation and growth or when studying external mixtures of particles of distinct sizes. However, such an effect is not expected to substantially influence the detection of ambient aerosols dominated by well-mixed accumulation mode particles.

Data availability. Data presented in this study can be obtained at the Zenodo online repository hosted by CERN (https://doi.org/10.5281/zenodo.5094651, Lee et al., 2021). Raw data can be obtained from the corresponding authors upon reasonable request.

Video supplement. Extractive electrospray ionization (EESI) enables online characterization of particle with negligible thermal and ionization-induced fragmentation. Our study elucidates the extraction mechanism between the particles and electrospray (ES) droplets of different properties. The results show that the extraction rate is likely affected by the coagulation rate between the particles and ES droplets, causing an increase in sensitivity by 1–3 orders of magnitude as particle size decreased from 300 to 30 nm. This size-dependent sensitivity is especially relevant when EESI is used to probe size-varying particles as is the case in aerosol formation and growth studies with size ranges below 100 nm. However, once coagulated, the particles undergo complete extraction within the ES droplet. For the video supplement, please see https://doi.org/10.5446/53709 (Lee, 2021).

Supplement. The supplement related to this article is available online at: https://doi.org/10.5194/amt-14-5913-2021-supplement.

Author contributions. CPL and MS designed the experiment. MS, CPL, DW, HL, MW, FA, VH and BL performed the experiments. CPL, MS, MW and FA analyzed the data. CPL, IEH, MS, DW, HL, JD, JGS, UB, DMB, NMD and ASHP interpreted the compiled results. CPL prepared the manuscript. All authors contributed to the discussion and revision of the manuscript.

Competing interests. The authors declare that they have no conflict of interest.

Disclaimer. Publisher's note: Copernicus Publications remains neutral with regard to jurisdictional claims in published maps and institutional affiliations.

Special issue statement. This article is part of the special issue "Simulation chambers as tools in atmospheric research (AMT/ACP/GMD inter-journal SI)". It is not associated with a conference.

Acknowledgements. We thank our technician Pascal Andre Schneider for technical support throughout our experiments and Martin Gysel for the scientific discussion. Special thanks to the CLOUD collaboration and CERN facilities for providing us the possibilities and resources to realize our investigation.

Financial support. This research has been supported by Horizon 2020 (grant nos. PSI-FELLOW-II-3i (grant no. 701647), EUROCHAMP-2020 (grant no. 730997) and CLOUD-MOTION (grant no. 764991)), the Schweizerischer Nationalfonds zur Förderung der Wissenschaftlichen Forschung (grant nos. 20020_172602, BSSGI0_155846 and 20FI20_172622), and the National Science Foundation (grant nos. AGS1801574 and AGS1531284).

Review statement. This paper was edited by Pierre Herckes and reviewed by three anonymous referees.

References

Berndt, T., Böge, O., Stratmann, F., Heintzenberg, J., and Kulmala, M.: Rapid formation of sulfuric acid particles at near-atmospheric conditions, Science, 307, 698–700, https://doi.org/10.1126/science.1104054, 2005.

Burnett, R., Chen, H., Szyszkowicz, M., Fann, N., Hubbell, B., Pope, C. A., Apte, J. S., Brauer, M., Cohen, A., Weichenthal, S., Coggins, J., Di, Q., Brunekreef, B., Frostad, J., Lim, S. S., Kan, H., Walker, K. D., Thurston, G. D., Hayes, R. B., Lim, C. C., Turner, M. C., Jerrett, M., Krewski, D., Gapstur, S. M., Diver, W. R., Ostro, B., Goldberg, D., Crouse, D. L., Martin, R. V., Peters, P., Pinault, L., Tjepkema, M., Van Donkelaar, A., Villeneuve, P. J., Miller, A. B., Yin, P., Zhou, M., Wang, L., Janssen, N. A. H., Marra, M., Atkinson, R. W., Tsang, H., Thach, T. Q., Cannon, J. B., Allen, R. T., Hart, J. E., Laden, F., Cesaroni, G., Forastiere, F., Weinmayr, G., Jaensch, A., Nagel, G., Concin, H., and Spadaro, J. V.: Global estimates of mortality associated with longterm exposure to outdoor fine particulate matter, P. Natl. Acad. Sci. USA, 115, 9592–9597, https://doi.org/10.1073/pnas.1803222115, 2018.

Chen, H., Venter, A., and Cooks, R. G.: Extractive electrospray ionization for direct analysis of undiluted urine, milk and other complex mixtures without sample preparation, Chem. Commun., 2042–2044, https://doi.org/10.1039/b602614a, 2006.

Cheng, C. Y., Yuan, C. H., Cheng, S. C., Huang, M. Z., Chang, H. C., Cheng, T. L., Yeh, C. S., and Shiea, J.: Electrospray-assisted laser desorption/ionization mass spectrometry for continuously monitoring the states of ongoing chemical reactions in organic or aqueous solution under ambient conditions, Anal. Chem., 80, 7699–7705, https://doi.org/10.1021/ac800952e, 2008.

Clarke, A. G., Willison, M. J., and Zeki, E. M.: Aerosol Neutralization by Atmospheric Ammonia, in: Commission of the European Communities, edited by: Versino, B., Physico-Chemical Behaviour of Atmospheric Pollutants, Springer, Dordrecht, 331–338, 1984.

Daellenbach, K. R., Uzu, G., Jiang, J., Cassagnes, L. E., Leni, Z., Vlachou, A., Stefenelli, G., Canonaco, F., Weber, S., Segers, A., Kuenen, J. J. P., Schaap, M., Favez, O., Albinet, A., Aksoyoglu, S., Dommen, J., Baltensperger, U., Geiser, M., El Haddad, I., Jaffrezo, J. L., and Prévôt, A. S. H.: Sources of particulate-matter air pollution and its oxidative potential in Europe, Nature, 587, 414–419, https://doi.org/10.1038/s41586-020-2902-8, 2020.

Dias, A., Ehrhart, S., Vogel, A., Williamson, C., Almeida, J., Kirkby, J., Mathot, S., Mumford, S., and Onnela, A.: Temperature uniformity in the CERN CLOUD chamber, Atmos. Meas. Tech., 10, 5075–5088, https://doi.org/10.5194/amt-10-5075-2017, 2017.

Ditto, J. C., Joo, T., Slade, J. H., Shepson, P. B., Ng, N. L., and Gentner, D. R.: Nontargeted Tandem Mass Spectrometry Analysis Reveals Diversity and Variability in Aerosol Functional Groups across Multiple Sites, Seasons, and Times of Day, Environ. Sci. Technol. Lett., 7, 60–69, https://doi.org/10.1021/acs.estlett.9b00702, 2020.

Donahue, N. M., Epstein, S. A., Pandis, S. N., and Robinson, A. L.: A two-dimensional volatility basis set: 1. organic-aerosol mixing thermodynamics, Atmos. Chem. Phys., 11, 3303–3318, https://doi.org/10.5194/acp-11-3303-2011, 2011.

Eichler, P., Müller, M., D'Anna, B., and Wisthaler, A.: A novel inlet system for online chemical analysis of semi-volatile submicron particulate matter, Atmos. Meas. Tech., 8, 1353–1360, https://doi.org/10.5194/amt-8-1353-2015, 2015.

George, I. J. and Abbatt, J. P. D.: Heterogeneous oxidation of atmospheric aerosol particles by gas-phase radicals, Nat. Chem., 2, 713–722, https://doi.org/10.1038/nchem.806, 2010.

Giannoukos, S., Lee, C. P., Tarik, M., Ludwig, C., Biollaz, S., Lamkaddam, H., Baltensperger, U., Henry Prevot, A. S., and Slowik, J.: Real-Time Detection of Aerosol Metals Using Online Extractive Electrospray Ionization Mass Spectrometry, Anal. Chem., 92, 1316–1325, https://doi.org/10.1021/acs.analchem.9b04480, 2020.

Hoffmann, T., Odum, J. R., Bowman, F., Collins, D., Klockow, D., Flagan, R. C., and Seinfeld, J. H.: Formation of organic aerosols from the oxidation of biogenic hydrocarbons, J. Atmos. Chem., 26, 189–222, https://doi.org/10.1023/A:1005734301837, 1997.

Holzinger, R., Williams, J., Herrmann, F., Lelieveld, J., Donahue, N. M., and Röckmann, T.: Aerosol analysis using a Thermal-Desorption Proton-Transfer-Reaction Mass Spectrometer (TD-PTR-MS): a new approach to study processing of organic aerosols, Atmos. Chem. Phys., 10, 2257–2267, https://doi.org/10.5194/acp-10-2257-2010, 2010.

Jimenez, J. L., Canagaratna, M. R., Donahue, N. M., Prevot, A. S. H., Zhang, Q., Kroll, J. H., DeCarlo, P. F., Allan, J. D., Coe, H., Ng, N. L., Aiken, A. C., Docherty, K. S., Ulbrich, I. M., Grieshop, A. P., Robinson, A. L., Duplissy, J., Smith, J. D., Wilson, K. R., Lanz, V. A., Hueglin, C., Sun, Y. L., Tian, J., Laaksonen, A., Raatikainen, T., Rautiainen, J., Vaattovaara, P., Ehn, M., Kulmala, M., Tomlinson, J. M., Collins, D. R., Cubison, M. J., Dunlea, E. J., Huffman, J. A., Onasch, T. B., Alfarra, M. R., Williams, P. I., Bower, K., Kondo, Y., Schnei-

der, J., Drewnick, F., Borrmann, S., Weimer, S., Demerjian, K., Salcedo, D., Cottrell, L., Griffin, R., Takami, A., Miyoshi, T., Hatakeyama, S., Shimono, A., Sun, J. Y., Zhang, Y. M., Dzepina, K., Kimmel, J. R., Sueper, D., Jayne, J. T., Herndon, S. C., Trimborn, A. M., Williams, L. R., Wood, E. C., Middlebrook, A. M., Kolb, C. E., Baltensperger, U., and Worsnop, D. R.: Evolution of organic aerosols in the atmosphere, Science, 326, 1525–1529, https://doi.org/10.1126/science.1180353, 2009.

Kalberer, M., Paulsen, D., Sax, M., Steinbacher, M., Dommen, J., Prevot, A. S. H., Fisseha, R., Weingartner, E., Frankevich, V., Zenobi, R., and Baltensperger, U.: Identification of Polymers as Major Components of Atmospheric Organic Aerosols, Science, 303, 1659–1662, https://doi.org/10.1126/science.1092185, 2004.

Kebarle, P. and Verkcerk, U. H.: Electrospray: From Ions in solution to Ions in the gas phase, what we know now, Mass Spectrom. Rev., 28, 898–917, https://doi.org/10.1002/mas.20247, 2009.

Kebarle, P. and Verkerk, U. H.: On the Mechanism of Electrospray Ionization Mass Spectrometry (ESIMS), in: Electrospray and MALDI Mass Spectrometry: Fundamentals, Instrumentation, Practicalities, and Biological Applications, edited by: Cole, R. B., John Wiley & Sons Inc., 82, 1–48, 2012.

Kirkby, J., Curtius, J., Almeida, J., Dunne, E., Duplissy, J., Ehrhart, S., Franchin, A., Gagné, S., Ickes, L., Kürten, A., Kupc, A., Metzger, A., Riccobono, F., Rondo, L., Schobesberger, S., Tsagkogeorgas, G., Wimmer, D., Amorim, A., Bianchi, F., Breitenlechner, M., David, A., Dommen, J., Downard, A., Ehn, M., Flagan, R. C., Haider, S., Hansel, A., Hauser, D., Jud, W., Junninen, H., Kreissl, F., Kvashin, A., Laaksonen, A., Lehtipalo, K., Lima, J., Lovejoy, E. R., Makhmutov, V., Mathot, S., Mikkilä, J., Minginette, P., Mogo, S., Nieminen, T., Onnela, A., Pereira, P., Petäjä, T., Schnitzhofer, R., Seinfeld, J. H., Sipilä, M., Stozhkov, Y., Stratmann, F., Tomé, A., Vanhanen, J., Viisanen, Y., Vrtala, A., Wagner, P. E., Walther, H., Weingartner, E., Wex, H., Winkler, P. M., Carslaw, K. S., Worsnop, D. R., Baltensperger, U., and Kulmala, M.: Role of sulphuric acid, ammonia and galactic cosmic rays in atmospheric aerosol nucleation, Nature, 476, 429–435, https://doi.org/10.1038/nature10343, 2011.

Kirkby, J., Duplissy, J., Sengupta, K., Frege, C., Gordon, H., Williamson, C., Heinritzi, M., Simon, M., Yan, C., Almeida, J., Trostl, J., Nieminen, T., Ortega, I. K., Wagner, R., Adamov, A., Amorim, A., Bernhammer, A. K., Bianchi, F., Breitenlechner, M., Brilke, S., Chen, X., Craven, J., Dias, A., Ehrhart, S., Flagan, R. C., Franchin, A., Fuchs, C., Guida, R., Hakala, J., Hoyle, C. R., Jokinen, T., Junninen, H., Kangasluoma, J., Kim, J., Krapf, M., Kurten, A., Laaksonen, A., Lehtipalo, K., Makhmutov, V., Mathot, S., Molteni, U., Onnela, A., Perakyla, O., Piel, F., Petaja, T., Praplan, A. P., Pringle, K., Rap, A., Richards, N. A. D., Riipinen, I., Rissanen, M. P., Rondo, L., Sarnela, N., Schobesberger, S., Scott, C. E., Seinfeld, J. H., Sipila, M., Steiner, G., Stozhkov, Y., Stratmann, F., Tomé, A., Virtanen, A., Vogel, A. L., Wagner, A. C., Wagner, P. E., Weingartner, E., Wimmer, D., Winkler, P. M., Ye, P., Zhang, X., Hansel, A., Dommen, J., Donahue, N. M., Worsnop, D. R., Baltensperger, U., Kulmala, M., Carslaw, K. S., and Curtius, J.: Ion-induced nucleation of pure biogenic particles, Nature, 533, 521–526, https://doi.org/10.1038/nature17953, 2016.

Konermann, L., Ahadi, E., Rodriguez, A. D., and Vahidi, S.: Unraveling the mechanism of electrospray ionization, Anal. Chem., 85, 2–9, https://doi.org/10.1021/ac302789c, 2013.

Kumbhani, S., Longin, T., Wingen, L. M., Kidd, C., Perraud, V., and Finlayson-Pitts, B. J.: New Mechanism of Extractive Electrospray Ionization Mass Spectrometry for Heterogeneous Solid Particles, Anal. Chem., 90, 2055–2062, https://doi.org/10.1021/acs.analchem.7b04164, 2018.

Law, W. S., Wang, R., Hu, B., Berchtold, C., Meier, L., Chen, H., and Zenobi, R.: On the mechanism of extractive electrospray ionization, Anal. Chem., 82, 4494–4500, https://doi.org/10.1021/ac100390t, 2010.

Lee, C. P.: Effects of Aerosol Size and Coating Thickness on the Molecular Detection using Extractive Electrospray Ionization, TIB AV-Portal [video supplement], https://doi.org/10.5446/53709, 2021.

Lee, C. P., Riva, M., Wang, D., Tomaz, S., Li, D., Perrier, S., Slowik, J. G., Bourgain, F., Schmale, J., Prevot, A. S. H., Baltensperger, U., George, C., and El Haddad, I.: Online Aerosol Chemical Characterization by Extractive Electrospray Ionization-Ultrahigh-Resolution Mass Spectrometry (EESI-Orbitrap), Environ. Sci. Technol., 54, 3871–3880, https://doi.org/10.1021/acs.est.9b07090, 2020.

Lee, C. P., Surdu, M., Bell, D. M., Lamkaddam, H., Wang, M., Ataei, F., Hofbauer, V., Lopez, B., Donahue, N. M., Dommen, J., Prevot, A. S. H., Slowik, J. G., Wang, D., Baltensperger, U., and El Haddad, I.: Effects of Aerosol Size and Coating Thickness on the Molecular Detection using Extractive Electrospray Ionization, Zenodo [data set], https://doi.org/10.5281/zenodo.5094651, 2021.

Lopez-Hilfiker, F. D., Mohr, C., Ehn, M., Rubach, F., Kleist, E., Wildt, J., Mentel, Th. F., Lutz, A., Hallquist, M., Worsnop, D., and Thornton, J. A.: A novel method for online analysis of gas and particle composition: description and evaluation of a Filter Inlet for Gases and AEROsols (FIGAERO), Atmos. Meas. Tech., 7, 983–1001, https://doi.org/10.5194/amt-7-983-2014, 2014.

Lopez-Hilfiker, F. D., Pospisilova, V., Huang, W., Kalberer, M., Mohr, C., Stefenelli, G., Thornton, J. A., Baltensperger, U., Prevot, A. S. H., and Slowik, J. G.: An extractive electrospray ionization time-of-flight mass spectrometer (EESI-TOF) for online measurement of atmospheric aerosol particles, Atmos. Meas. Tech., 12, 4867–4886, https://doi.org/10.5194/amt-12-4867-2019, 2019.

Marquez, C. A., Wang, H., Fabbretti, F., and Metzger, J. O.: Electron-transfer-catalyzed dimerization of trans-anethole: Detection of the distonic tetramethylene radical cation intermediate by extractive electrospray ionization mass spectrometry, J. Am. Chem. Soc., 130, 17208–17209, https://doi.org/10.1021/ja806791c, 2008.

Meier, L., Schmid, S., Berchtold, C., and Zenobi, R.: Contribution of liquid-phase and gas-phase ionization in extractive electrospray ionization mass spectrometry of primary amines, Eur. J. Mass Spectrom., 17, 345–351, https://doi.org/10.1255/ejms.1146, 2011.

Molteni, U., Bianchi, F., Klein, F., El Haddad, I., Frege, C., Rossi, M. J., Dommen, J., and Baltensperger, U.: Formation of highly oxygenated organic molecules from aromatic compounds, Atmos. Chem. Phys., 18, 1909–1921, https://doi.org/10.5194/acp-18-1909-2018, 2018.

Müller, M., Eichler, P., D'Anna, B., Tan, W., and Wisthaler, A.: Direct Sampling and Analysis of Atmospheric Particulate Organic Matter by Proton-Transfer-Reaction

Mass Spectrometry, Anal. Chem., 89, 10889–10897, https://doi.org/10.1021/acs.analchem.7b02582, 2017.

Pagonis, D., Campuzano-Jost, P., Guo, H., Day, D. A., Schueneman, M. K., Brown, W. L., Nault, B. A., Stark, H., Siemens, K., Laskin, A., Piel, F., Tomsche, L., Wisthaler, A., Coggon, M. M., Gkatzelis, G. I., Halliday, H. S., Krechmer, J. E., Moore, R. H., Thomson, D. S., Warneke, C., Wiggins, E. B., and Jimenez, J. L.: Airborne extractive electrospray mass spectrometry measurements of the chemical composition of organic aerosol, Atmos. Meas. Tech., 14, 1545–1559, https://doi.org/10.5194/amt-14-1545-2021, 2021.

Seinfeld, J. H. and Pandis, S. N.: Atmospheric Chemistry and Physics: From Air Pollution to Climate Change, 3rd edn., Wiley-Interscience, Hoboken, 2016.

Simon, M., Dada, L., Heinritzi, M., Scholz, W., Stolzenburg, D., Fischer, L., Wagner, A. C., Kürten, A., Rörup, B., He, X.-C., Almeida, J., Baalbaki, R., Baccarini, A., Bauer, P. S., Beck, L., Bergen, A., Bianchi, F., Bräkling, S., Brilke, S., Caudillo, L., Chen, D., Chu, B., Dias, A., Draper, D. C., Duplissy, J., El-Haddad, I., Finkenzeller, H., Frege, C., Gonzalez-Carracedo, L., Gordon, H., Granzin, M., Hakala, J., Hofbauer, V., Hoyle, C. R., Kim, C., Kong, W., Lamkaddam, H., Lee, C. P., Lehtipalo, K., Leiminger, M., Mai, H., Manninen, H. E., Marie, G., Marten, R., Mentler, B., Molteni, U., Nichman, L., Nie, W., Ojdanic, A., Onnela, A., Partoll, E., Petäjä, T., Pfeifer, J., Philippov, M., Quéléver, L. L. J., Ranjithkumar, A., Rissanen, M. P., Schallhart, S., Schobesberger, S., Schuchmann, S., Shen, J., Sipilä, M., Steiner, G., Stozhkov, Y., Tauber, C., Tham, Y. J., Tomé, A. R., Vazquez-Pufleau, M., Vogel, A. L., Wagner, R., Wang, M., Wang, D. S., Wang, Y., Weber, S. K., Wu, Y., Xiao, M., Yan, C., Ye, P., Ye, Q., Zauner-Wieczorek, M., Zhou, X., Baltensperger, U., Dommen, J., Flagan, R. C., Hansel, A., Kulmala, M., Volkamer, R., Winkler, P. M., Worsnop, D. R., Donahue, N. M., Kirkby, J., and Curtius, J.: Molecular understanding of new-particle formation from α-pinene between -50 and $+25\,^{\circ}$C, Atmos. Chem. Phys., 20, 9183–9207, https://doi.org/10.5194/acp-20-9183-2020, 2020.

Stark, H., Yatavelli, R. L. N., Thompson, S. L., Kang, H., Krechmer, J. E., Kimmel, J. R., Palm, B. B., Hu, W., Hayes, P. L., Day, D. A., Campuzano-Jost, P., Canagaratna, M. R., Jayne, J. T., Worsnop, D. R., and Jimenez, J. L.: Impact of Thermal Decomposition on Thermal Desorption Instruments: Advantage of Thermogram Analysis for Quantifying Volatility Distributions of Organic Species, Environ. Sci. Technol., 51, 8491–8500, https://doi.org/10.1021/acs.est.7b00160, 2017.

Tavakoli, F. and Olfert, J. S.: An instrument for the classification of aerosols by particle relaxation time: Theoretical models of the aerodynamic aerosol classifier, Aerosol Sci. Technol., 47, 916–926, https://doi.org/10.1080/02786826.2013.802761, 2013.

Tavakoli, F. and Olfert, J. S.: Determination of particle mass, effective density, mass-mobility exponent, and dynamic shape factor using an aerodynamic aerosol classifier and a differential mobility analyzer in tandem, J. Aerosol Sci., 75, 35–42, https://doi.org/10.1016/j.jaerosci.2014.04.010, 2014.

Tavakoli, F., Symonds, J. P. R., and Olfert, J. S.: Generation of a monodisperse size-classified aerosol independent of particle charge, Aerosol Sci. Technol., 48, i–iv, https://doi.org/10.1080/02786826.2013.877121, 2014.

Tröstl, J., Chuang, W. K., Gordon, H., Heinritzi, M., Yan, C., Molteni, U., Ahlm, L., Frege, C., Bianchi, F., Wagner, R., Simon, M., Lehtipalo, K., Williamson, C., Craven, J. S., Duplissy, J., Adamov, A., Almeida, J., Bernhammer, A. K., Breitenlechner, M., Brilke, S., Dias, A., Ehrhart, S., Flagan, R. C., Franchin, A., Fuchs, C., Guida, R., Gysel, M., Hansel, A., Hoyle, C. R., Jokinen, T., Junninen, H., Kangasluoma, J., Keskinen, H., Kim, J., Krapf, M., Kürten, A., Laaksonen, A., Lawler, M., Leiminger, M., Mathot, S., Möhler, O., Nieminen, T., Onnela, A., Petäjä, T., Piel, F. M., Miettinen, P., Rissanen, M. P., Rondo, L., Sarnela, N., Schobesberger, S., Sengupta, K., Sipilä, M., Smith, J. N., Steiner, G., Tomè, A., Virtanen, A., Wagner, A. C., Weingartner, E., Wimmer, D., Winkler, P. M., Ye, P., Carslaw, K. S., Curtius, J., Dommen, J., Kirkby, J., Kulmala, M., Riipinen, I., Worsnop, D. R., Donahue, N. M., and Baltensperger, U.: The role of low-volatility organic compounds in initial particle growth in the atmosphere, Nature, 533, 527–531, https://doi.org/10.1038/nature18271, 2016.

Wagner, A. C., Bergen, A., Brilke, S., Fuchs, C., Ernst, M., Hoker, J., Heinritzi, M., Simon, M., Bühner, B., Curtius, J., and Kürten, A.: Size-resolved online chemical analysis of nanoaerosol particles: a thermal desorption differential mobility analyzer coupled to a chemical ionization time-of-flight mass spectrometer, Atmos. Meas. Tech., 11, 5489–5506, https://doi.org/10.5194/amt-11-5489-2018, 2018.

Wang, R., Gröhn, A. J., Zhu, L., Dietiker, R., Wegner, K., Günther, D., and Zenobi, R.: On the mechanism of extractive electrospray ionization (EESI) in the dual-spray configuration, Anal. Bioanal. Chem., 402, 2633–2643, https://doi.org/10.1007/s00216-011-5471-8, 2012.

Wingen, L. M. and Finlayson-Pitts, B. J.: Probing surfaces of atmospherically relevant organic particles by easy ambient sonic-spray ionization mass spectrometry (EASI-MS), Chem. Sci., 10, 884–897, https://doi.org/10.1039/c8sc03851a, 2019.

Yue, D., Hu, M., Wu, Z., Wang, Z., Guo, S., Wehner, B., Nowak, A., Achtert, P., Wiedensohler, A., Jung, J., Kim, Y. J. and Liu, S.: Characteristics of aerosol size distributions and new particle formation in the summer in Beijing, J. Geophys. Res., 114, D00G12, https://doi.org/10.1029/2008JD010894, 2009.

Supplement of Atmos. Meas. Tech., 14, 5913–5923, 2021
https://doi.org/10.5194/amt-14-5913-2021-supplement

Atmospheric Measurement Techniques
Open Access
EGU

Supplement of

Effects of aerosol size and coating thickness on the molecular detection using extractive electrospray ionization

Chuan Ping Lee et al.

Correspondence to: Imad El Haddad (imad.el-haddad@psi.ch), Dongyu Wang (dongyu.wang@psi.ch), and Jay G. Slowik (jay.slowik@psi.ch)

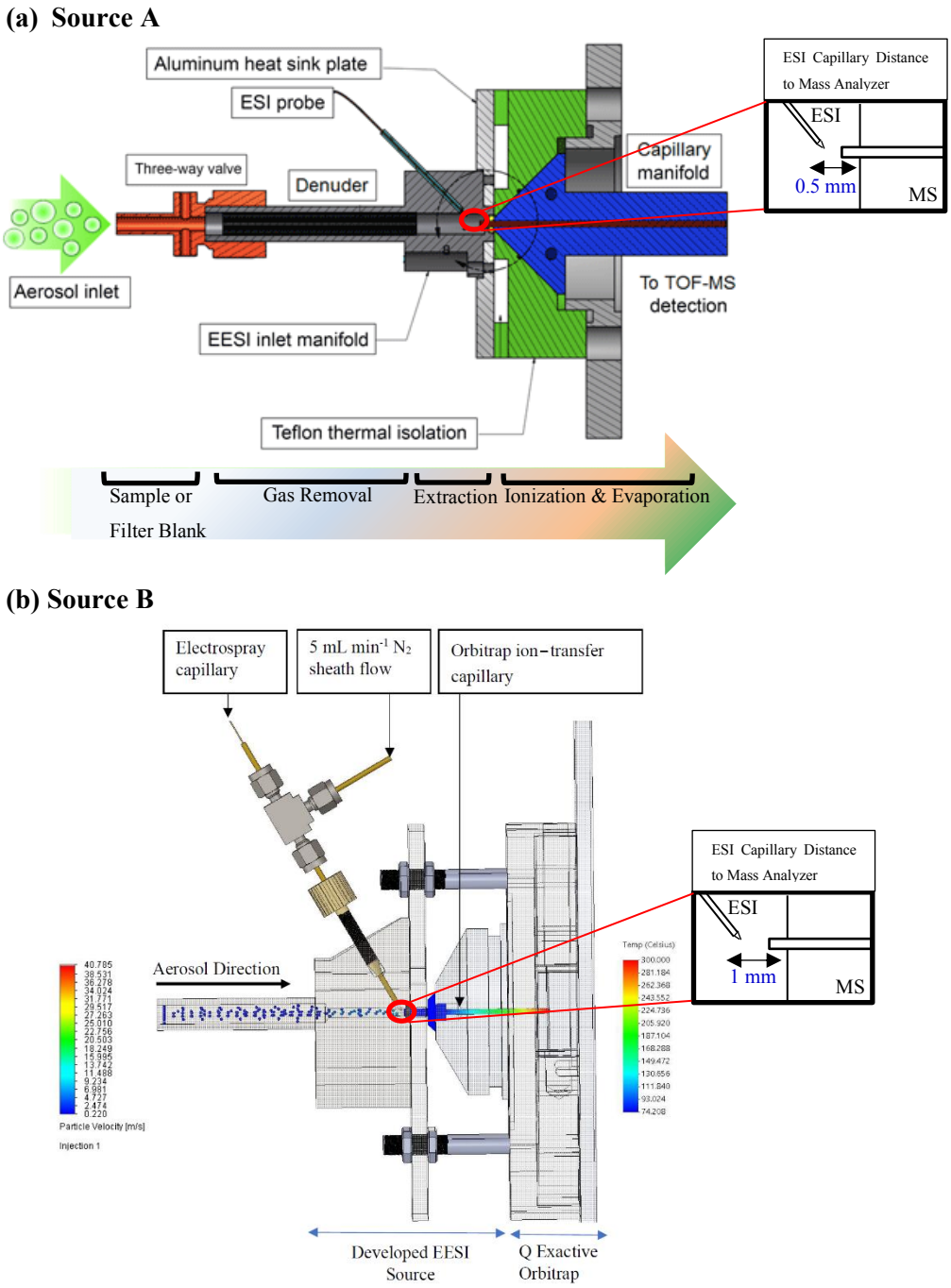

Figure S1. (a) EESI-TOF inlet compatible with the Tofwerk TOF system. (b) EESI-Orbitrap inlet compatible with the Thermo Fischer Scientific Orbitrap and Tofwerk TOF systems. Note: The charcoal denuder is not included in the picture (b). Source A was developed by the Laboratory of Atmospheric Chemistry, Paul Scherrer Institute, Switzerland (LAC-PSI) in collaboration with TOFWERK AG, Switzerland. Source B was development by LAC-PSI in collaboration with IRCELYON, France (Lopez-Hilfiker et al., 2019; Lee et al., 2020). The approximate distance between the tip of the spray capillary and the heated ion transfer tube at the mass spectrometer interface is shown in the insets. The ESI probes of the EESI sources have the similar inclination of 30° from the horizontal axis at the mass analyzer capillary. Both EESI sources were deployed on the same mass analyzer with the same sampling flow of 0.8 L min^{-1} for the whole experiment.

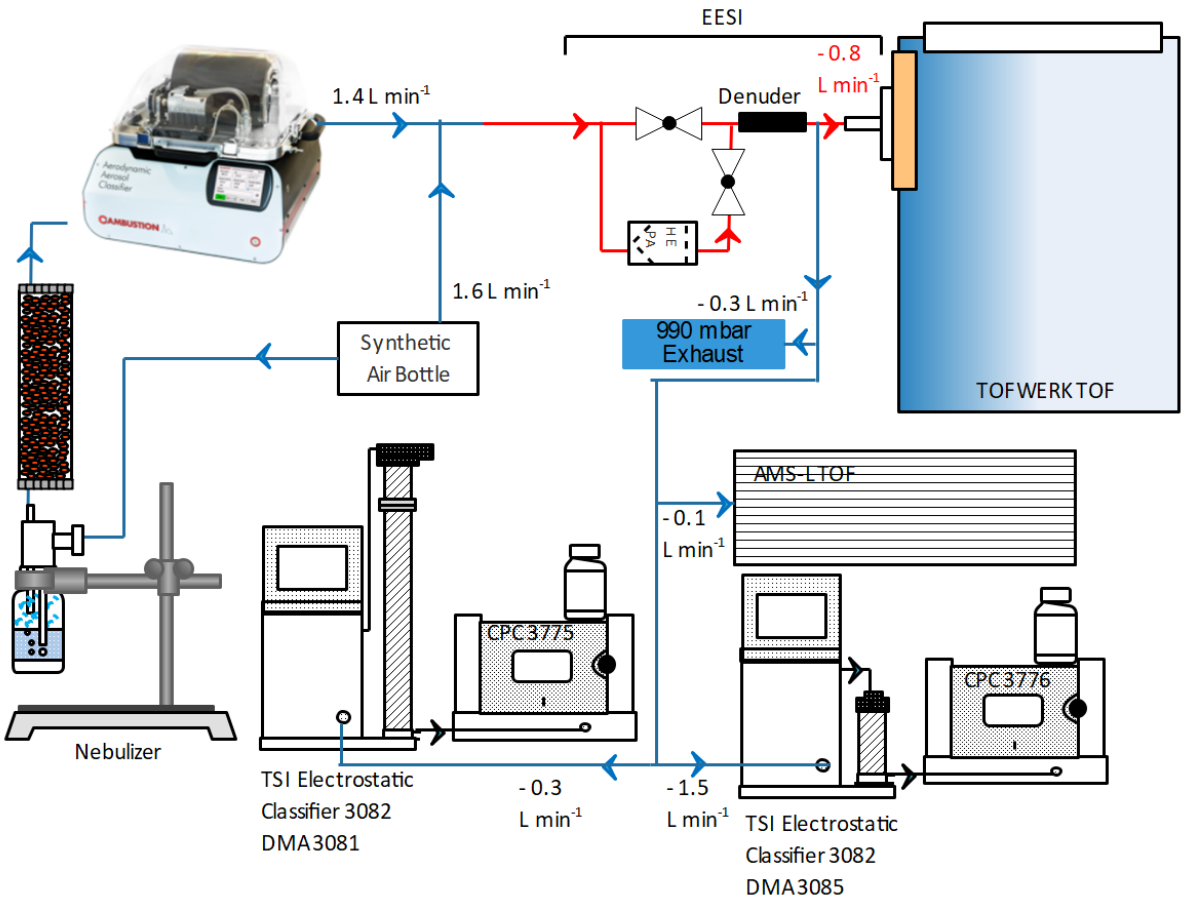

30 **Figure S2.** Schematic of the experimental setup for size-dependent sensitivity of the EESI-TOF. Red lines indicate the schematic layout of the EESI-TOF ionization inlet with additional two two-way valves and tubing manifolds prior to the electrospray ionization region for two different settings: (1) with charcoal denuder only and (2) with charcoal denuder and HEPA filter. Blue lines indicate the setup, which is used for the size-dependent sensitivity experiment.

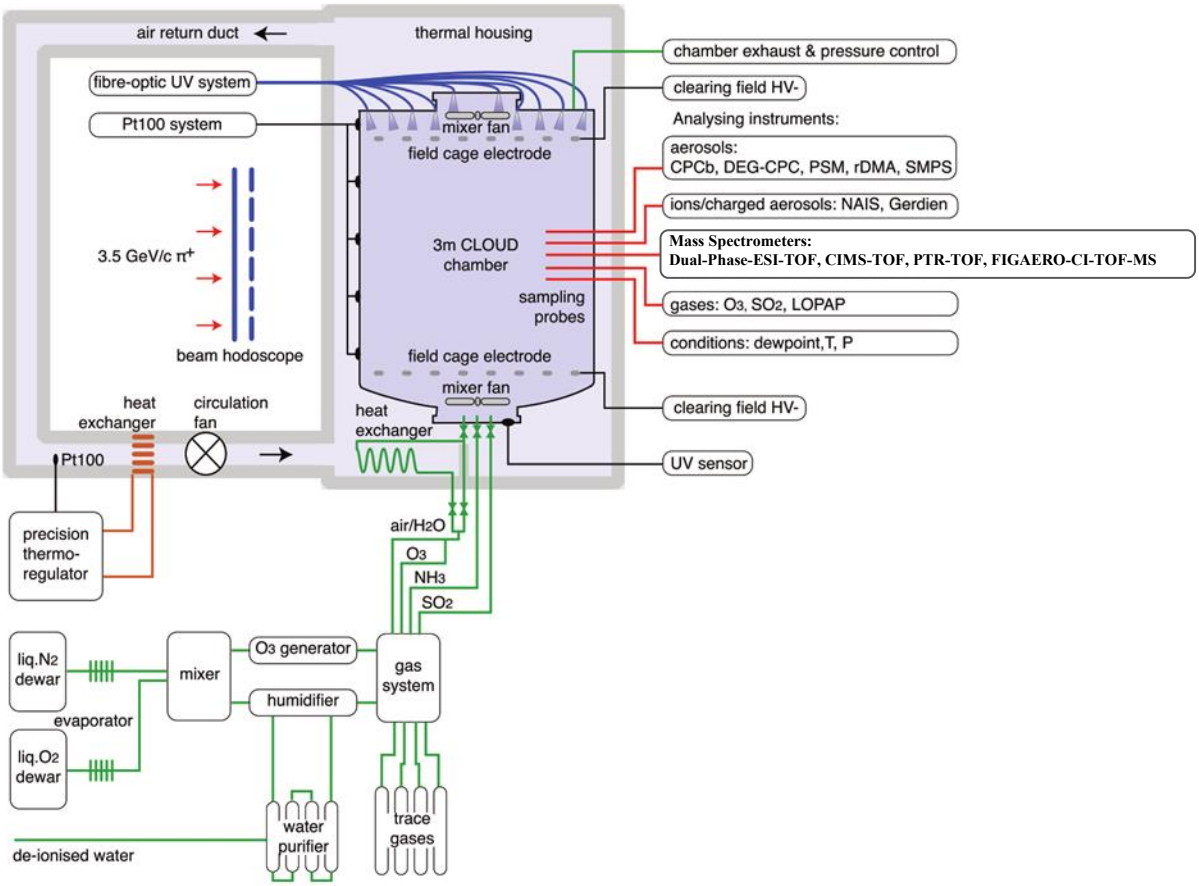

Figure S3. Schematic diagram of the CLOUD-14 experiment at CERN, modified from Kirkby et al. (2011).

CLOUD chamber. The CLOUD facility provides suitable conditions to study new particle formation (NPF) under atmospherically relevant conditions, using the well-characterized cylindrical stainless-steel chamber (CLOUD chamber) with ultra-low contamination level and equipped with state-of-the art instrumentation (see Figure S3). The CLOUD chamber is an electro-polished stainless-steel cylindrical chamber of 3 m diameter, ~4 m height and 26.1 m^3 inner volume, positioned inside a thermal housing (Kirkby et al., 2011). A continuous flow of synthetic air from evaporation of cryogenic liquid nitrogen and liquid oxygen at a volume mixing ratio of 79:21 is injected to the chamber to balance the experiment sample flow. When all the instruments are connected to the CLOUD facility, the total air flow rate is typically 270 L min^{-1}, resulting in a dilution lifetime of 1.6 h in the chamber. Humidity of the chamber is adjusted by passing the air through a Nafion® humidifier using ultrapure water (18 MΩ cm, Millipore Corporation).

The relative humidity of the chamber is determined by dew point mirrors (EdgeTech). Ozone (O_3) is generated by exposing a small fraction of the air through a quartz tube surrounded by UVC lamps (wavelength <240 nm) and added to the inlet chamber flow. For NPF experiments, the chamber is operated at 5 mbar above atmospheric pressure using a pressure regulated valve. Two counter-rotating stainless-steel fans are mounted on the roof and bottom of the chamber to enable a uniform mixing inside the chamber. Under typical NPF experimental conditions, the fans are operated with 12% fan speed, resulting in a wall loss lifetime of 0.002 s^{-1} for sulfuric acid. A typical experiment in CLOUD is running in continuous mode, so precursors are constantly injected into the chamber. An

experiment starts when the particle concentration inside the chamber is low enough for the measurement and precursor gases such as SO_2 and / or volatile organic compounds (VOCs) have reached the intended concentration. Chemical reactions start by turning on UV lights or by mixing VOCs with oxidants such as ozone.

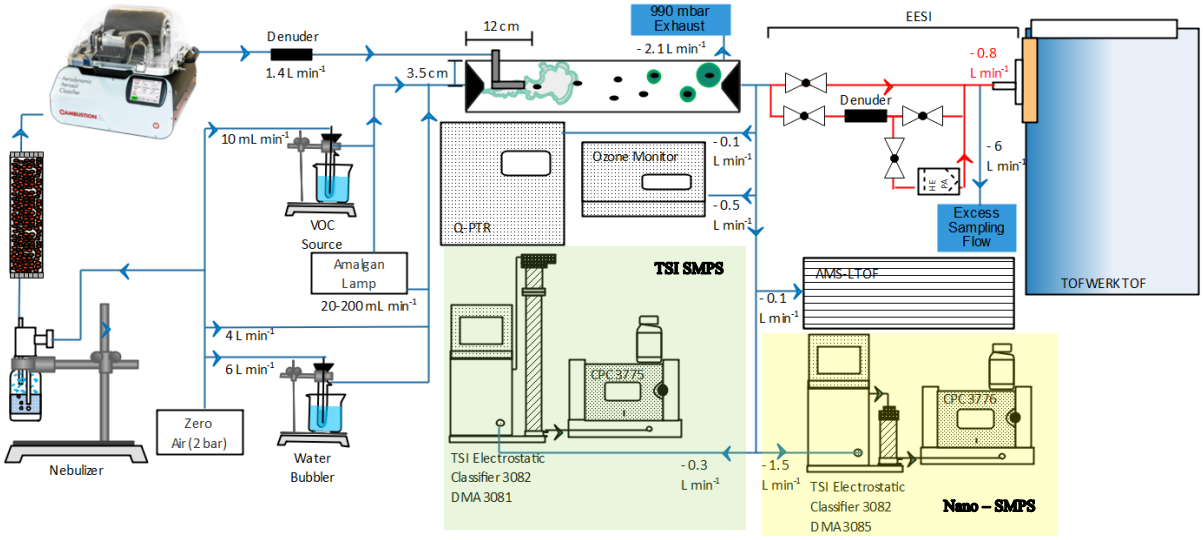

Figure S4. Schematic of the experimental setup for coating experiments using α-pinene oxidation products from a flow tube reactor. Inorganic particles (NH_4NO_3) are injected into the flow tube which act as condensation sink for the low-volatility oxidation products. Red lines indicate the schematic layout of the EESI-TOF ionization inlet with additional valve and tubing manifolds prior to the electrospray ionization region for three different settings: (1) open straight tube (without denuder and HEPA filter), (2) with charcoal denuder only, (3) with charcoal denuder and HEPA filter. Blue lines indicate the setup that is used for the coating experiment.

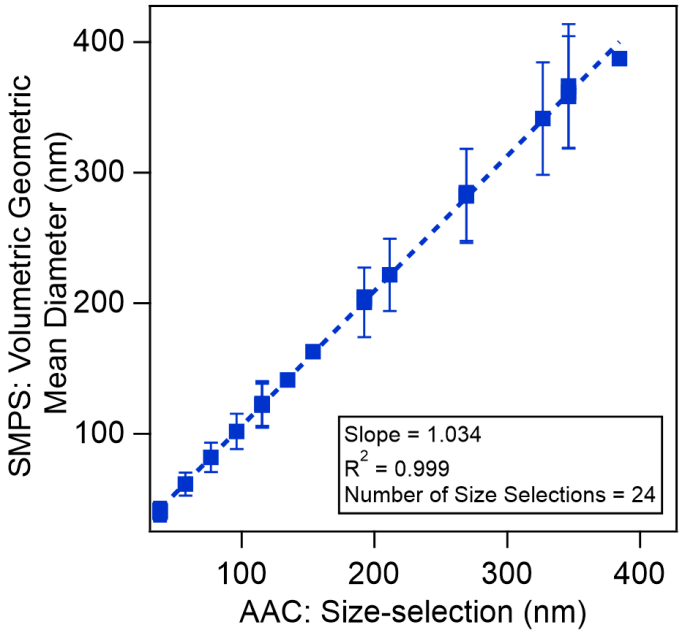

Figure S5. Measured volumetric geometric mean diameter by the SMPS as a function of selected size by the Aerosol Aerodynamic Classifier for levoglucosan particles. The SMPS measurement was corrected by applying the ion mobility ratio for air, which is 1.2/1.4. The AAC aerodynamic diameter was corrected according to the density of levoglucosan described below. The full width at half maximum (FWHM) of the measured particle size distribution by the SMPS is indicated by the *y*-axis uncertainty marker. The blue dotted-line indicates the linear fit with goodness of fit R^2 = 0.999.

For spherical particles, the aerodynamic diameter D_{ae} is defined as

$$D_{ae} = D_P \sqrt{\frac{\rho_P C_c(D_P)}{\rho_0 C_c(D_{ae})}} \quad \text{(Eq. S1)}$$

where $C_c(D)$ is the Cunningham slip correction factor applied to diameter D_p and D_{ae}, D_p is the diameter measured by a differential mobility particles sizer, ρ_0 = 1000 kg m^{-3} and ρ_P the density of the particle. To simplify the relationship shown in Figure S5,

$$\frac{D_P}{D_{ae}} = \sqrt{\frac{\rho_0}{\rho_P}} \quad \text{(Eq. S2)}$$

For the case of levoglucosan particles ρ_P = 1690 kg m^{-3}, the ratio of $\sqrt{\frac{\rho_0}{\rho_P}}$ = 0.769. After the correction of the aerodynamic diameters using levoglucosan density, the slope measured in Figure S5 is within an uncertainty of 5%.

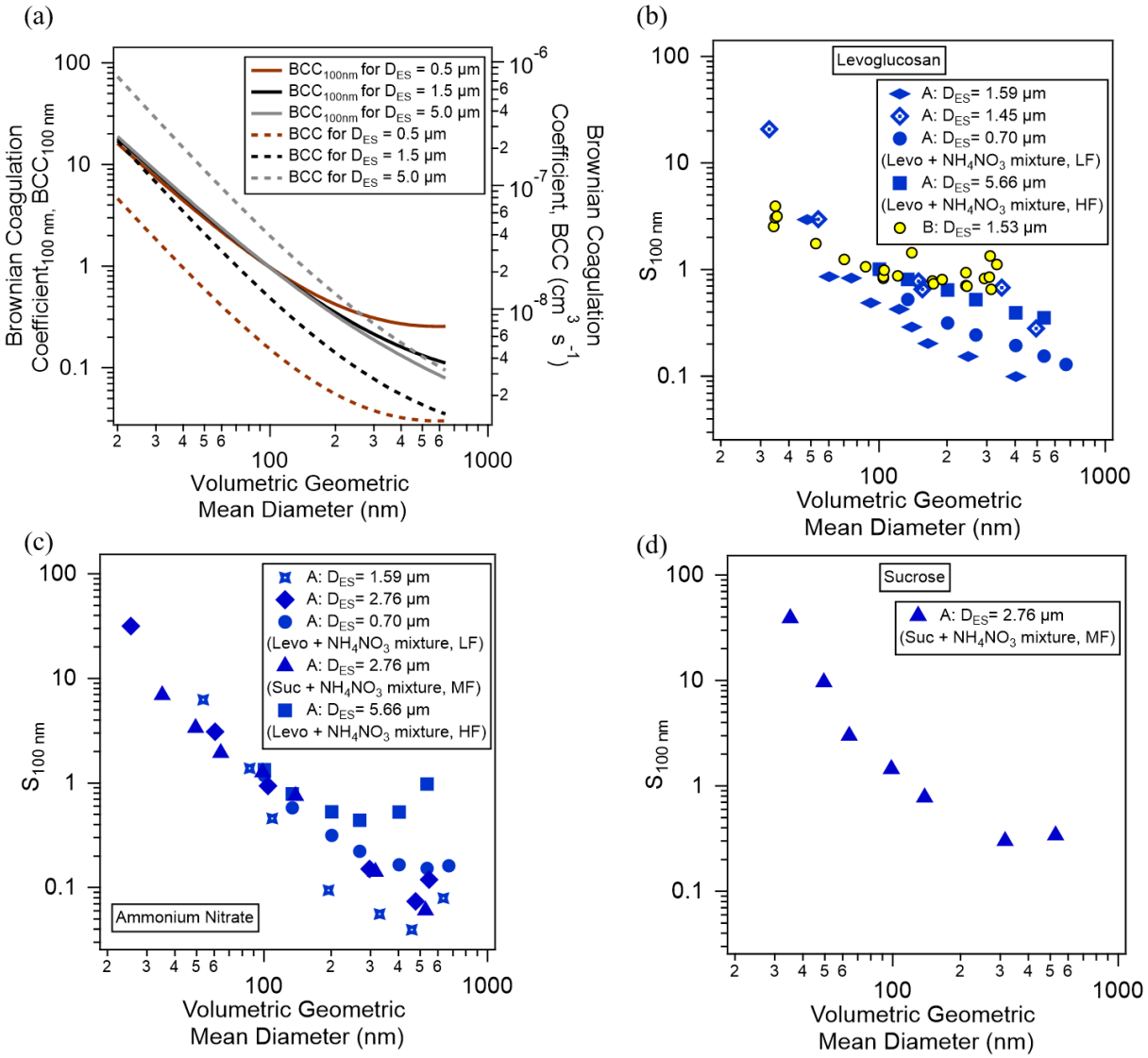

Figure S6. (a) Brownian coagulation coefficient (BCC) in cm^3 s^{-1} calculated assuming different parent electrospray droplet diameters (D_{ES}). The particle diameter is plotted along the *x*-axis. The D_{ES} values were chosen to cover the expected range (0.5 µm and 5.0 µm) and median (~1.5 µm) sizes of the actual electrospray droplet generated in this study (Table S3). D_{ES} is the electrospray parent droplet diameters that were estimated using scaling laws shown in Figure S7, assuming that the ES is operating in the Taylor cone jet mode (Gañán-Calvo et al., 2018). As done in-text for the measured sensitivities, the normalized BCC values (relative to that for 100 nm particle), BCC_{100nm} are also shown. (b-d) size-dependent sensitivity measurements using individual and internally-mixed (mixture) chemical standards, i.e. (b) levoglucosan, (c) NH_4NO_3 and (d) sucrose. A and B denote the types of the EESI source used as depicted in Figure S1. The estimated D_{ES} value for a given the experimental condition (Table S2) is also shown in the legends. LF, MF and HF denote low, medium and high ES capillary flow as tabulated in Table S2. The mass concentration for internally mixed levoglucosan and NH_4NO_3 particles with D_p > 100 nm were measured by an LTOF-AMS.

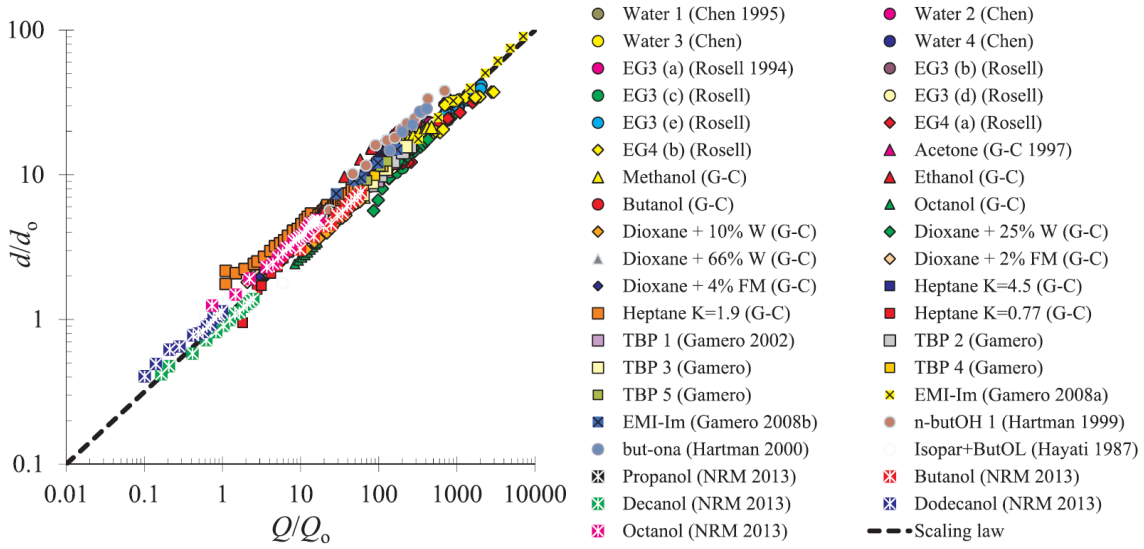

Figure S7. Scaling laws for predicting the orders of magnitude of the size d of the emitted ES charged droplet based on the flow rate Q for 39 types of electrospray working solutions. The predicted diameter d is denoted as $d = d_0\sqrt{Q/Q_0}$ (Gañán-Calvo et al., 2018).

D_{ES} shown in Figure S6 is calculated by from Q, Q_0 and d_0. Q is the calculated flow rate using the Hagen-Poiseuille equation:

$$Q = \frac{\Delta p \pi R^4}{8\mu L} \quad \text{(Eq. S3)}$$

where Δp is the pressure difference applied to the ES bottle reservoir, R is the inner radius of the ES capillary, L is the length of the ES capillary (80 cm) and μ is the dynamic viscosity of the ES working solution. The dynamic viscosity of H_2O:ACN (50:50 v/v) and H_2O at 25 ˚C are 0.65 and 0.89 mPa s, respectively. See Table S1 for other variables. Q_0 and d_0 are defined as

$$Q_0 = \sigma\varepsilon_0/(\rho K)$$
$$d_0 = [\sigma\varepsilon_0^2/\rho K^2]^{1/3} \quad \text{(Eq. S4)}$$

where σ is the surface tension, ρ is the density and K is the electrical conductivity of the electrospray working solutions.

Table S1. Physical properties of the electrospray solvents.

Physical Properties of the Electrospray Solvents			
Types of ES Solvent	Surface tension σ (N m^{-1})	Volumetric Density ρ (kg m^{-3})	Electrical Conductivity K (S m^{-1})
H_2O:ACN (50:50 v/v)	0.0514	842.54	0.000252
H_2O	0.072	997	0.0005

When all the variables are determined, D_{ES} is estimated as (Gañán-Calvo et al., 2016, 2018)

$$D_{ES} = d_0\sqrt{Q/Q_0}. \quad \text{(Eq. S5)}$$

Table S2. Size dependence experiments for different chemicals, EESI source and ES operating parameters. Levo#, AN# and Suc# indicate different levoglucosan, NH_4NO_3 and sucrose experiment runs, respectively.

Index no.	**EESI Source Designs**	**ES voltage (kV)**	**ES pressure (mbar)**	**ES capillary inner diameter (µm)**	**ES solution**	**Nebulization solution**	**ES Flow Rate, Q (nL min^{-1})**
Levo1 + AN1	A	2.6	200	50	H_2O:ACN (50:50 v/v)	Mixed	354
Levo2 + AN2	A	2.9	800	100	H_2O:ACN (50:50 v/v)	Mixed	22655
Levo3	A	2.95	200 - 400	75	H_2O:ACN (50:50 v/v)	Single	1792-3584
Levo4	A	2.88	200 - 400	75	H_2O	Single	1309-2617
AN3	A	2.95	200 - 400	75	H_2O:ACN (50:50 v/v)	Single	1792-3584
AN4 + Suc1	A	2.9	600	75	H_2O:ACN (50:50 v/v)	Mixed	5375
AN5	A	2.9	600	75	H_2O:ACN (50:50 v/v)	Single	5375
Levo5	B	2.8	120 - 250	75	H_2O:ACN (50:50 v/v)	Single	1075-2240
Levo6	B	3	120 - 250	75	H_2O:ACN (50:50 v/v)	Single	1075-2240
Levo7	B	3	120 - 250	75	H_2O:ACN (50:50 v/v)	Single	1075-2240
Levo8	B	2.9	120 - 250	75	H_2O:ACN (50:50 v/v)	Single	1075-2240
Levo9	B	2.9	120 - 250	75	H_2O:ACN (50:50 v/v)	Single	1075-2240

Table S3. Estimation of electrospray (ES) parent droplet size and number concentrations using the median of the ES flow rate. The estimated ES parent droplet number flux was used for the estimation of coagulation rates between ES droplets and particles.

Index no.	**ES Flow Rate, Q (nL min^{-1})**	**Estimated ES Parent Droplet Size, D_{ES} (μm)**	**Estimated ES Parent Droplet Number Flux N_{ES}, Q/D_{ES} (s^{-1})**
Levo1 + AN1	354	0.70	$32.9 \cdot 10^6$
Levo2 + AN2	22655	5.66	$4 \cdot 10^6$
Levo3	1792-3584	1.59	$14.2 - 28.3 \cdot 10^6$
Levo4	1309-2617	1.45	$13.7 - 27.3 \cdot 10^6$
AN3	1792-3584	1.59	$14.2 - 28.3 \cdot 10^6$
AN4 + Suc1	5375	2.76	$8.1 \cdot 10^6$
AN5	5375	2.76	$8.1 \cdot 10^6$
Levo5	1075-2240	1.53	$9.6 - 20 \cdot 10^6$
Levo6	1075-2240	1.53	$9.6 - 20 \cdot 10^6$
Levo7	1075-2240	1.53	$9.6 - 20 \cdot 10^6$
Levo8	1075-2240	1.53	$9.6 - 20 \cdot 10^6$
Levo9	1075-2240	1.53	$9.6 - 20 \cdot 10^6$

The coagulation coefficients K_{12} were calculated using the Fuchs form of the Brownian coagulation coefficient (Seinfeld and Pandis, 2016).

$$K_{12} = 2\pi(D_1 + D_2)(D_{p1} + D_{p2})\left(\frac{D_{p1}+D_{p2}}{D_{p1}+D_{p2}+2(g_1^2+g_2^2)^{1/2}} + \frac{8(D_1+D_2)}{(\bar{C}_1^2+\bar{C}_2^2)^{\frac{1}{2}}(D_{p1}+D_{p2})}\right)^{-1} \quad \text{(Eq. S6)}$$

where

$$\bar{C}_i = \left(\frac{8k_BT}{\pi m_i}\right)^{1/2}$$

$$l_i = \frac{8D_i}{\pi\bar{C}_i}$$

$$g_i = \frac{\sqrt{2}}{3D_{pi}l_i}\left[\left(D_{pi} + l_i\right)^3 - \left(D_{pi}^2 + l_i^2\right)^{3/2}\right] - D_{pi}$$

$$D_i = \frac{k_BTC_c}{3\pi\mu D_{pi}},$$

and C_c is the Cunningham slip correction factor. D_{p1} is denoted as D_{ES} (Eq. S5, Table S3) with the density of the electrospray solution (Table S1) and D_{p2} is denoted as the mid-size of the measured j-th bin of the size-selected particle size distribution with the density of the particle. For clarity, K_{12} is hereafter referred to as $K_{ES,J}$.

The coagulation rate J_{12} between the ES parent droplets and analyte particles can be calculated as

$$J_{12} = N_{ES}\sum_{j=1}^{\infty} K_{ES,J}N_J \quad \text{(Eq. S7)}$$

where N_{ES} is the estimated ES parent droplet number flux (Table S3), $K_{ES,J}$ is the calculated Brownian coagulation coefficient (Eq. S6) and N_j is the number concentration of the measured j-th bin of the size-selected analyte particle size distribution. Please note that Eq. S7 does not take into account of potential inhomogeneity of ES droplet and particle distributions during coagulation.

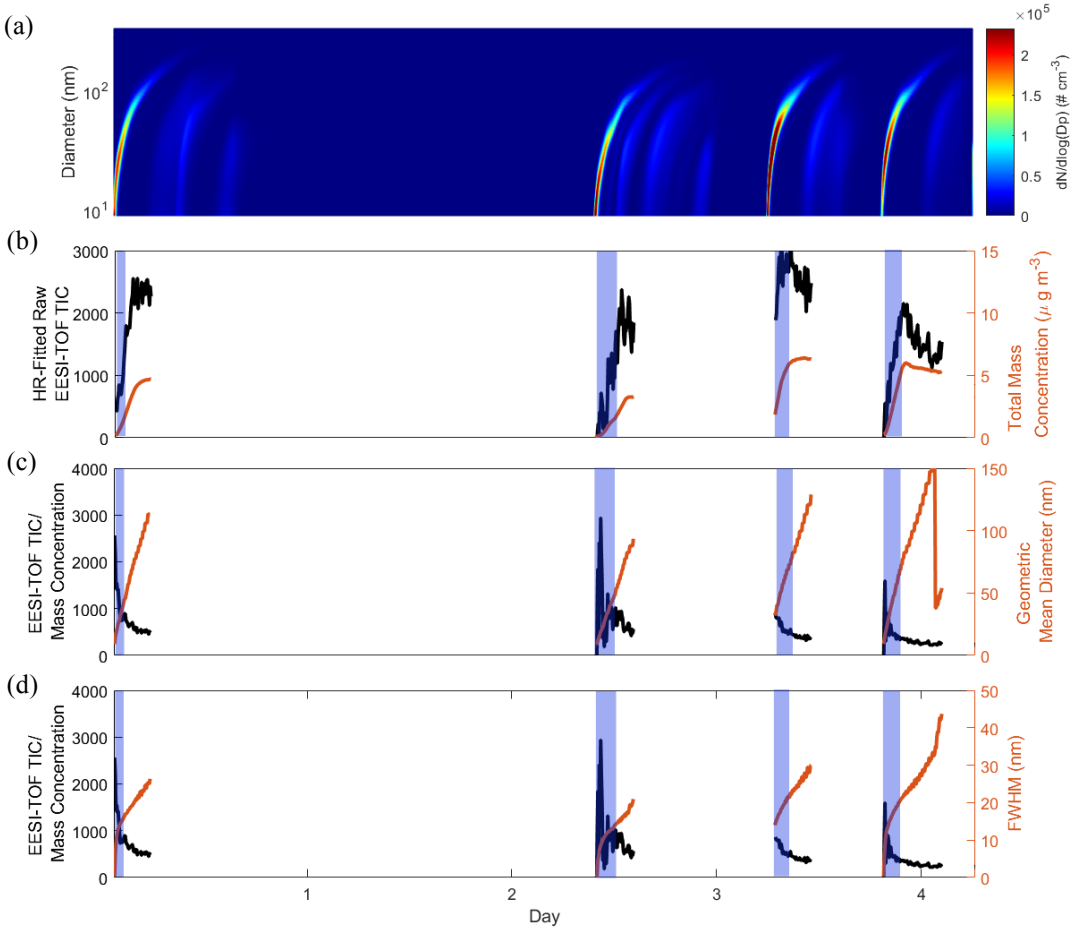

Figure S8. SOA formation experiments in the CLOUD chamber. (a) SMPS measurements of the number-weighted size distribution. (b) Raw EESI-TOF total ion counts (TIC) after high-resolution peak fitting and total mass concentrations measured by the SMPS with an effective mass density of 1.3 g cm^{-3}. (c) EESI-TOF TIC normalized by the mass concentration measured by the SMPS, and the geometric mean diameter. (d) EESI-TOF TIC normalized by the mass concentration measured by the SMPS, and the full width at half maximum (FWHM) of the volume-weighted size distribution. Shaded areas depict the period during new particle formation events where EESI size-dependent sensitivities are observed as shown in Figure 3.

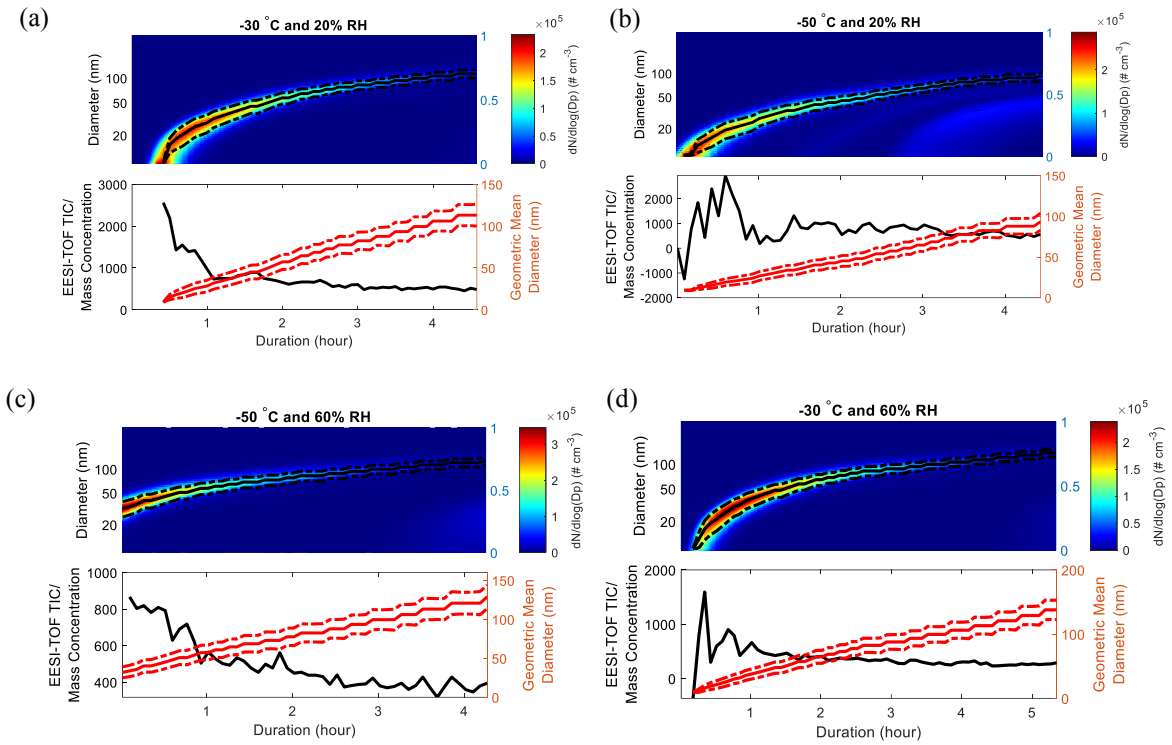

Figure S9. (Top sub-panel) SMPS size distributions and (bottom sub-panel) sum of the high-resolution fitted ions of EESI normalized by the mass concentration measured by the SMPS for α-pinene (AP) SOA formation experiments in the CLOUD chamber at four different conditions. (a) AP SOA formation at -30 °C and 20% relative humidity (RH). (b) AP SOA formation at -50 °C and 20% RH. (c) AP SOA formation at -50 °C and 60% RH. (d) AP SOA formation at -30 °C and 60% RH.

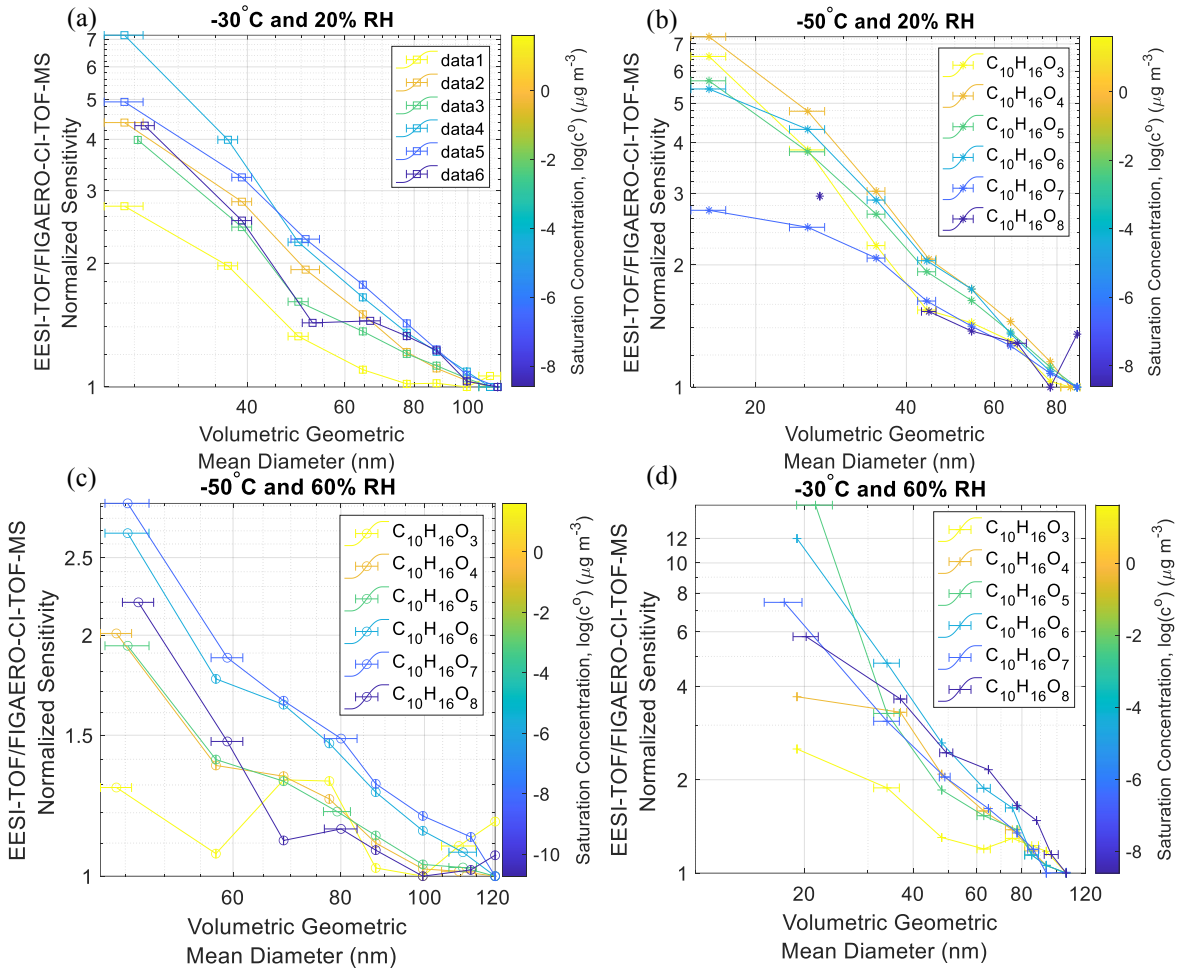

Figure S10. Measurements of $C_{10}H_{16}O_{3\text{-}8}$ in the particle phase. EESI-TOF to FIGAERO-CI-TOF-MS normalized sensitivity for AP SOA formation experiments in the CLOUD chamber at four different conditions.

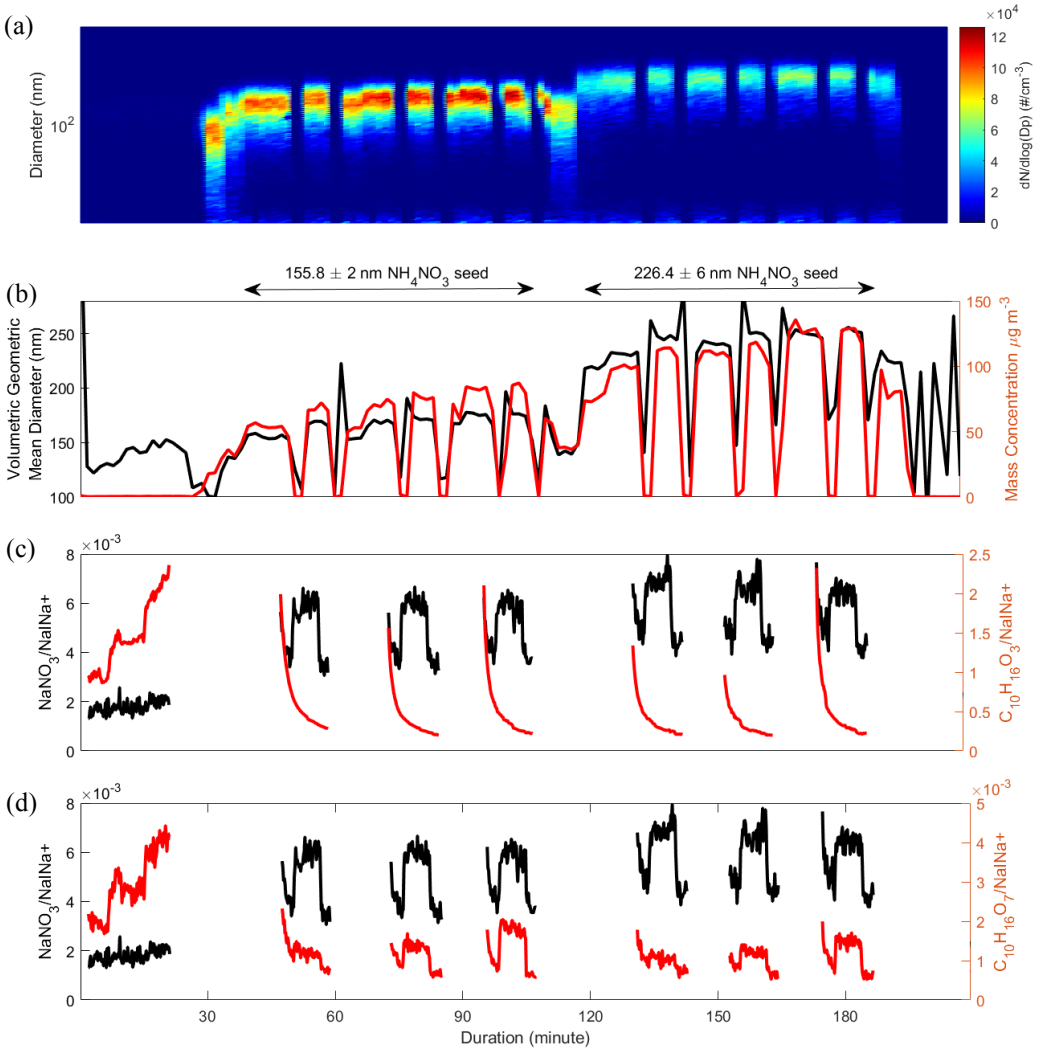

Figure S11. Coating of NH_4NO_3 particles using oxidation products of α-pinene ozonolysis. (a) Size distribution of the coated NH_4NO_3 particles. (b) Volume weighted geometric mean diameter and mass concentration measured by the SMPS. (c) Signals of NH_4NO_3 particles and particle-phase $C_{10}H_{16}O_3$ molecules. (d) Signals of NH_4NO_3 particles and particle-phase $C_{10}H_{16}O_8$ molecules.

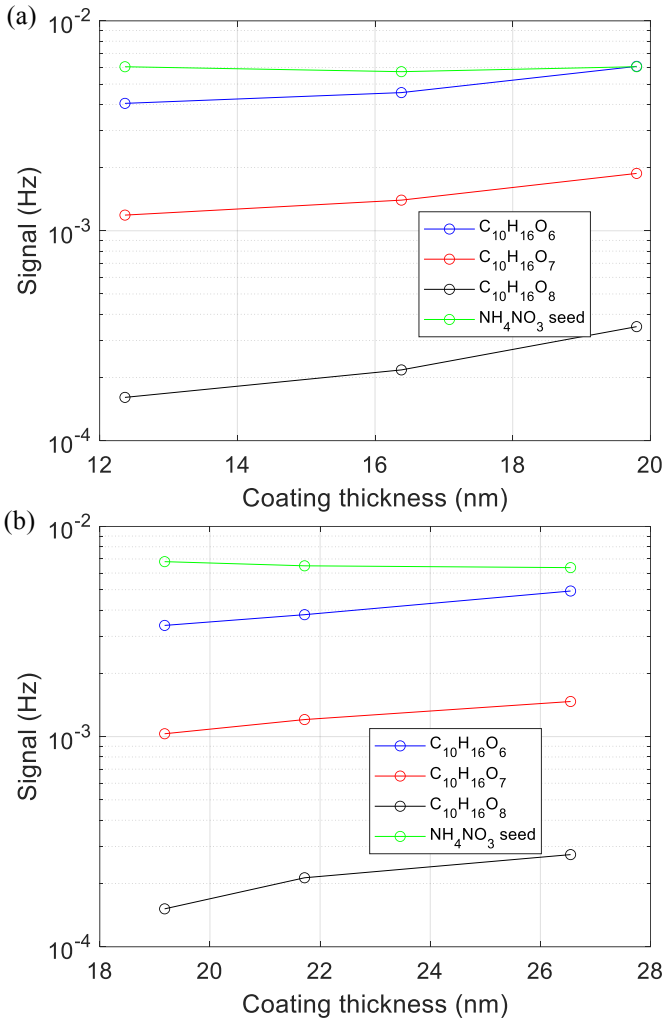

Figure S12. Absolute changes of NH_4NO_3 and $C_{10}H_{16}O_{6\text{-}8}$ as a function of the coating thickness for two different NH_4NO_3 particle core sizes of (a) 156 nm and (b) 226 nm after normalization to the most abundant electrospray ion adduct $[NaI+Na]^+$.

References

Gañán-Calvo, A. M., López-Herrera, J. M., Rebollo-Muñoz, N. and Montanero, J. M.: The onset of electrospray: The universal scaling laws of the first ejection, Sci. Rep., 6(1), 1–9, doi:10.1038/srep32357, 2016.

Gañán-Calvo, A. M., López-Herrera, J. M., Herrada, M. A., Ramos, A. and Montanero, J. M.: Review on the physics of electrospray: From electrokinetics to the operating conditions of single and coaxial Taylor cone-jets, and AC electrospray, J. Aerosol Sci., 125, 32–56, doi:10.1016/j.jaerosci.2018.05.002, 2018.

Kirkby, J., Curtius, J., Almeida, J., Dunne, E., Duplissy, J., Ehrhart, S., Franchin, A., Gagné, S., Ickes, L., Kürten, A., Kupc, A., Metzger, A., Riccobono, F., Rondo, L., Schobesberger, S., Tsagkogeorgas, G., Wimmer, D., Amorim, A., Bianchi, F., Breitenlechner, M., David, A., Dommen, J., Downard, A., Ehn, M., Flagan, R. C., Haider, S., Hansel, A., Hauser, D., Jud, W., Junninen, H., Kreissl, F., Kvashin, A., Laaksonen, A., Lehtipalo, K., Lima, J., Lovejoy, E. R., Makhmutov, V., Mathot, S., Mikkilä, J., Minginette, P., Mogo, S., Nieminen, T., Onnela, A., Pereira, P., Petäjä, T., Schnitzhofer, R., Seinfeld, J. H., Sipilä, M., Stozhkov, Y., Stratmann, F., Tomé, A., Vanhanen, J., Viisanen, Y., Vrtala, A., Wagner, P. E., Walther, H., Weingartner, E., Wex, H., Winkler, P. M., Carslaw, K. S., Worsnop, D. R., Baltensperger, U. and Kulmala, M.: Role of sulphuric acid, ammonia and galactic cosmic rays in atmospheric aerosol nucleation, Nature, 476(7361), 429–435, doi:10.1038/nature10343, 2011.

Lee, C. P., Riva, M., Wang, D., Tomaz, S., Li, D., Perrier, S., Slowik, J. G., Bourgain, F., Schmale, J., Prevot, A. S. H., Baltensperger, U., George, C. and El Haddad, I.: Online Aerosol Chemical Characterization by Extractive Electrospray Ionization-Ultrahigh-Resolution Mass Spectrometry (EESI-Orbitrap), Environ. Sci. Technol., 54(7), 3871–3880, doi:10.1021/acs.est.9b07090, 2020.

Lopez-Hilfiker, Pospisilova, V., Huang, W., Kalberer, M., Mohr, C., Stefenelli, G., Thornton, J. A., Baltensperger, U., Prevot, A. S. H. and Slowik, J. G.: An extractive electrospray ionization time-of-flight mass spectrometer (EESI-TOF) for online measurement of atmospheric aerosol particles, Atmos. Meas. Tech., 12(9), 4867–4886, doi:10.5194/amt-12-4867-2019, 2019.

Seinfeld, J. H. and Pandis, S. N.: Atmospheric Chemistry and Physics: From Air Pollution to Climate Change, 3rd ed., Wiley., 2016.